

MODELLING AND CONTROL OF 3 DOF ROBOTIC SYSTEM AND DC-DC CONVERTERS

A DISSERTATION
SUBMITTED IN PARTIAL FULFILLMENT OF THE
REQUIREMENTS FOR THE AWARD OF THE DEGREE
OF

MASTER OF TECHNOLOGY

IN

CONTROL & INSTRUMENTATION

SUBMITTED BY

TIASHA JASH

(2K23/C&I/06)

UNDER SUPERVISION OF

PROF. BHARAT BHUSHAN



DEPARTMENT OF ELECTRICAL ENGINEERING

DELHI TECHNOLOGICAL UNIVERSITY

(Formerly Delhi College of Engineering)

Shahbad Daulatpur, Main Bawana Road, Delhi-110042, India

MAY, 2025

ACKNOWLEDGEMENT

I would like to express my heartfelt gratitude to my supervisor, Prof. Bharat Bhushan, for his invaluable guidance, unwavering support, and continuous encouragement throughout the course of this work. His insightful suggestions, constructive feedback, and prompt assistance at every stage were instrumental in shaping this project and enriching my learning experience.

I am deeply grateful to the Department of Electrical Engineering, Delhi Technological University (DTU), for providing me with the opportunity to undertake this project work as part of my M.Tech curriculum. The academic environment, resources, and infrastructure offered by the department played a pivotal role in facilitating my research and project execution.

I would like to extend my sincere thanks to all the faculty members and staff of the Control Systems Laboratory, Department of Electrical Engineering, DTU, for their technical assistance, cooperation, and motivation during the course of this work.

I am equally thankful to my fellow peers and colleagues whose discussions and shared experiences contributed positively to the development of this project.

Finally, I would like to acknowledge the unwavering support and inspiration of my family and friends. Their faith in my abilities and constant encouragement gave me the strength to pursue and complete my M.Tech at this advanced stage of my academic journey.

Place: Delhi
Date: May 2025

Tiasha Jash
2K23/C&I/06
M.Tech (Control and Instrumentation)
Delhi Technological University



DELHI TECHNOLOGICAL UNIVERSITY

(Formerly Delhi College of Engineering)

Bawana Road, Delhi-110042

CANDIDATE'S DECLARATION

I, **Tiasha Jash**, Roll No. 2K23/C&I/06, M.Tech. (Control & Instrumentation), hereby declare that the project Dissertation titled “**MODELLING AND CONTROL OF 3 DOF ROBOTIC SYSTEM AND DC-DC CONVERTERS**” which is submitted by me to the Department of Electrical Engineering, Delhi Technological University, Delhi in partial fulfillment of the requirement for the award of the degree of Master of Technology, is not imitated from any source without proper citation and is authentic. This work has not beforehand formed the root for the award of any Degree, Diploma, Fellowship, Associateship or any other similar title or acknowledgment.

Place- Delhi

Date: May 2015

Tiasha Jash

2K23/C&I/06



DELHI TECHNOLOGICAL UNIVERSITY

(Formerly Delhi College of Engineering)

Bawana Road, Delhi-110042

CERTIFICATE BY SUPERVISOR

I, hereby certify that the Dissertation titled “**Modelling and Control of 3 DOF Robotic System and DC-DC Converters**” which is submitted by **Tiasha Jash**, 2K23/C&I/06, Department of Electrical Engineering, Delhi Technological University, Delhi in partial fulfillment of the requirement for the award of the degree of Master of Technology in **Control and Instrumentation** is a testimony of the project work carried out by the student under my supervision. To the best of my awareness this work has not been submitted in part or full for any Degree or Diploma to any University.

Place: Delhi

Date: May 2025

Prof. Bharat Bhushan

(Prof. EED, DTU)

ABSTRACT

This research presents a comprehensive investigation into the implementation and comparative analysis of various control strategies applied to two different yet control-sensitive systems: a 3-degree-of-freedom (3-DOF) haptic device and DC-DC converters specifically buck, boost, and SEPIC topologies used in renewable energy applications. Despite their different domains, both systems require robust control solutions to achieve precision, stability, and dynamic performance under varying conditions. For the haptic device, accurate position control and smooth user interaction are critical, particularly in applications such as surgical simulation, virtual reality, and remote manipulation. In this study, Proportional-Integral (PI) and Proportional-Integral-Derivative (PID) controllers are employed to regulate the position of the end-effector. These classical control strategies are evaluated for their effectiveness in tracking performance, settling time, and stability in the presence of mechanical nonlinearities and dynamic changes. Simulation results validate the applicability of these controllers in achieving stable and responsive behaviour. In contrast, the DC-DC converters utilized in renewable energy systems require control strategies capable of managing nonlinear behaviour, maintaining output voltage regulation, and reducing transient effects under variable input and load conditions. To address these requirements, this work applies PID, Fuzzy Logic controller (FLC) and Adaptive Neuro-Fuzzy Inference System (ANFIS) controllers. Each controller is assessed based on its ability to improve performance and ensure efficient power conversion across different operating conditions. The comparative analysis reveals that while classical controllers such as PI and PID provide acceptable performance in both systems, intelligent control techniques particularly Fuzzy Logic and ANFIS offer superior adaptability, learning capability, and robustness for the nonlinear and time-varying nature of power electronic converters. The study concludes that selecting an appropriate control strategy based on system dynamics, control objectives, and performance criteria is crucial for enhancing system efficiency, reliability, and responsiveness in both haptic and renewable energy domains.

TABLE OF CONTENTS

ACKNOWLEDGEMENT	i
CANDIDATE’S DECLARATION	ii
CERTIFICATE BY SUPERVISOR	iii
ABSTRACT	iv
TABLE OF CONTENTS	v
LIST OF FIGURES	vii
LISTS OF TABLES	ix
 CHAPTER 1-INTRODUCTION	
1.1 Robotic Technology in Control Systems	1
1.2 Haptic Device	1
1.3 Literature Review of Robotic System	2
1.4 Role of DC-DC Converters	3
1.5 Literature Review of DC-DC Converters	4
1.6 Outline of Dissertation	5
 CHAPTER 2 -3 DOF ROBOTIC SYSTEM – STRUCTURE, OPERATION, AND KINEMATICS	
2.1 OMNI Bundle	6
2.2 System Specifications	6
2.3 Robotic Kinematics	8
2.3.1. Forward Kinematics (FK)	8
2.3.2. Inverse Kinematics (IK)	10
2.4 Position Control and Path Tracking	11
2.5 Applications of the OMNI Haptic Device	12
2.6 Advantages of the OMNI Haptic Device	12
2.7 Conclusions	12
 CHAPTER 3-DC-DC CONVERTERS – OPERATION, MODELLING AND APPLICATION	
3.1 DC-DC Converters	13
3.2 Buck Converter	14
3.3 Boost Converter	17

3.4	SEPIC Converter	19
3.5	Conclusions	22
CHAPTER 4-CONTROL METHODOLOGIES		
4.1	Open Loop VS Close Loop	23
4.2	Types of Controller	23
4.3	Classical PID Controller	24
4.4	Fuzzy Logic Control System (FLC)	24
4.5	ANFIS	26
4.6	Layers of ANFIS	26
4.7	Learning Algorithm of ANFIS	27
4.8	Conclusions	28
Chapter 5-HARDWARE RESULTS OF ROBOTIC SYSTEM		
5.1	Robotic System	29
5.2	Forward and Inverse Kinematics Analysis	29
5.3	Position Control	31
5.4	Path Tracking	36
5.5	Conclusions	39
CHAPTER 6-DC- DC CONVERTERS SIMULATION RESULTS		
6.1	Buck Converter	40
6.2	Boost converter	45
6.3	SEPIC Converter	49
CHAPTER 7-HARDWARE IMPLEMENTATION OF BUCK CONVERTER		
7.1	BUCK CONVERTER SIMULATION ON KICAD	52
7.2	Buck converter Hardware setup	53
7.3	Gate driving circuit using 555 timer	55
CHAPTER 8-CONCLUSIONS & FUTURE SCOPE		
8.1	Conclusions	59
8.2	Future Scope	60
REFERENCES		61
LIST OF PUBLICATIONS		64

LIST OF FIGURES

Figure no.	Description	Page No.
Fig.2.1	Omni haptic device	6
Fig.2.2	Board	7
Fig.2.3	Links & stylus	7
Fig.2.4	IF ,FK	10
Fig.2.5	PID block diagram	11
Fig.3.1	Basic buck converter	14
Fig.3.2	Off mode operation	15
Fig.3.3	CCM/DCM	17
Fig.3.4	Basic boost converter	17
Fig.3.5	On mode boost working	18
Fig.3.6	Sepic converter	19
Fig.3.7	Mode 1 operation	20
Fig.4.1	Open loop	23
Fig.4.2	Close loop	23
Fig.4.3	Block diagram PID	24
Fig.4.4	FLC system	25
Fig.4.5	ANFIS layers	26
Fig.5.1	Omni hardware setup	31
Fig.5.2	PID robotic system	31
Fig.5.3	Joint 1 position control	33
Fig.5.4	Velocity graph	33
Fig.5.5	Joint 2 position control	35
Fig.5.6	Joint 3 position control	36
Fig.5.7	Path tracking	38
Fig. 6.1	FLC implementation	41
Fig. 6.2	Anfis implementation	41
Fig.6.3	ANFIS model structure	42
Fig.6.4	Open loop Buck	42
Fig 6.5	FLC Buck	43

Fig.6.6	PID buck	43
Fig.6.7	ANFIS buck	44
Fig.6.8	Voltage output of buck	44
Fig 6.9	Open loop boost	46
Fig.6.10	PID boost	46
Fig.6.11	FLC boost	46
Fig.6.12	ANFIS boost	47
Fig.6.13	Voltage output boost	47
Fig.6.14	Open loop sepic	49
Fig.6.15	PID SEPIC	49
Fig.6.16	FLC SEPIC	50
Fig.6.17	ANFIS sepic	50
Fig.6.18	Voltage output of SEPIC	50
Fig.7.1	Buck converter on KICAD	54
Fig.7.2	Hardware setup	54
Fig.7.3	Toroidal inductor	55
Fig.7.4	555 timer	56
Fig.7.5	Astable mode results	58

LISTS OF TABLES

Table no.	Table title	Page No.
Table 2.1	System specification of omni	8
Table 2.2	D-H parameter	9
Table 3.1	CCM/DCM comparison	17
Table 5.1	FK results	29
Table 5.2	IK results	30
Table 5.3	Joint 1 control	32
Table 5.4	Joint 2 control	34
Table 5.5	Joint 3 control	35
Table 6.1	Buck converter specifications	42
Table 6.2	Buck results analysis	45
Table 6.3	Boost converter specifications	45
Table 6.4	Boost results analysis	48
Table 6.5	SEPIC specifications	49
Table 6.6	SEPIC results analysis	51
Table 7.1	Hardware components of buck converter	53
Table 7.2	Gate triggering description	56

CHAPTER 1

INTRODUCTION

1.1 Robotic Technology in Control Systems

Robotics is a multidisciplinary science that amalgamates mechanical engineering, electronics, computer science, and control systems to produce intelligent devices—robots—that act in an autonomous or semi-autonomous manner. Although the idea traces back to ancient and medieval automata, contemporary robotics emerged with the creation of Unimate in the 1950s, revolutionizing industrial automation. Progress in computers, sensors, and artificial intelligence has allowed robots to progress from simple machines to perceptive, decision-making, and adaptive intelligent systems. They are now an integral part of manufacturing, healthcare, defense, home automation, and space exploration. In recent times, the addition of machine learning has made it possible to create cognitive robotics—autonomous robots that learn and get better with time—increasing their application in dynamic, unstructured environments

1.2 Haptic Device

Robotics is important not just for technological progress but also for defining the future of society, the economy, and work. With the increasing role of robots in everyday life, it becomes important to realize how they are constructed, operated, and their overall influence. Haptics, which is based on the Greek term haptikos (or "touch"), is the science of touch interaction between man and machine. Haptics draws concepts from biochemistry, psychology, neurology, engineering, and computer science to investigate how touch is used to transfer information between the physical and virtual worlds. Haptic technology produces sensations of touch through the application of forces or pressure against the skin, enabling users to perceive virtual objects. Touch in humans consists of skin sensors, nerves, and brain processing to interpret the world. Haptic systems in machines are composed of sensors, mechanics, and algorithms that mimic the process. The main purpose of haptics is to monitor forces on the body and decipher the messages they send. Haptic software software computes where and how the touch happens, giving instant feedback. In robotics, haptics makes it possible for machines to feel their surroundings and offer touch feedback to users. This enables robots to move more smoothly, recognize objects, and interact with humans more naturally.

1.3 Literature Review of Robotic System

Haptic devices are now part of a new way of learning, giving users the chance to feel motion and haptic data in a virtual environment. This project explains the fundamentals of haptic technology, says what devices are used in this area and points out key haptic technologies. During the investigation and analysis, the author discovered that haptic learning is used in classrooms, on printed pages, in games, handouts and digital media, for all different school subjects and teaching levels. The main topic of this section is the actuator, specifically solenoid actuators, piezo-actuators, electroactive polymers, ultrasonic actuators and MR fluids.[1]Recent advances in software and hardware have made it possible to study haptics and motions, allowing people to communicate with virtual three-dimensional objects by gesture or touch. These tools play an important part in education. If gestures and tactile innovation are part of chemistry teaching, learners may more easily learn concepts related to many chemical sciences. An introduction to a gesture control method used for visualising and modelling chemistry experiments with molecules.[2]Haptic technologies for studying social touch are discussed in the article. The study of social interaction in psychology and neuroscience is very engaging.

Now, with new technology, it is now much easier for people to socialize apart from one another and with artificial agents. Work in social touch inspired researchers to learn how similar interactions can occur online and they have found that there are online tools with emotional intensity equal to real touch. A summary of recent work on social touch development, research ideas for the next application phase and tips for practitioners add to the overall paper. [4] Touch forms one of the most important types of sensory feedback a surgeon receives during surgery. Even so, scientific research into haptics (kinaesthetic and tactile methods) in clinical education is scarce. Recording and expressing haptic feedback is difficult which limits this basic understanding. The emphasis of this chapter is on applying haptics to advance robotized and remote treatments and to train doctors and nurses. It outlines what haptic feedback systems are available currently and how haptic cues might contribute to the growth of surgical skills. An overview and outline of various haptic interfaces is included within the medical operations section[5].

Current touch-based systems are possible thanks to haptic technology which lets users feel and sense changes in the digital world. Many different tasks are now possible using interactivity created by haptics devices such as robots, training professionals and entertainment systems. Doctors and others in healthcare can improve their skills without danger by using virtual tissue sensation during practice. Robotics manipulator control starts with kinematic analysis where users need forward and inverse kinematics for their operations. The process of end-effector position determination using specified joint angles is known as forward kinematics while inverse kinematics calculates joint variable values for defined end-effector positions. The inverse kinematics problems of 3-degree-of-freedom (3-DOF) robotic manipulators received improved trajectory accuracy[1,2] implemented their neuro-fuzzy intelligent solution, Then forward kinematics formulated via Denavit-

Hartenberg (D-H) convention and added Sliding Mode Controller (SMC) for better trajectory tracking[3].

The Phantom OMNI haptic device analysis for its robotic applications where the researchers examined both its kinematic operations and manipulability functionality. The device became more suitable for teleoperation and medical simulation due to their improved modelling of position and velocity tracking. The Phantom OMNI series haptic devices supply electromechanical feedback systems for medical diagnostics and rehabilitation along with teleoperation activities. Surgical training benefit from haptic integration because it provides accurate touch-based feedback that enhances medical professional education. Precise remote control of robotic equipment through haptic feedback remains vital for maintaining objects in unsafe conditions such as space exploration and nuclear plant tasks[4-7]. A Sliding Mode Controller (SMC) constitutes one of the primary controllers in haptic teleoperation while maintaining stability against disturbances and uncertainties. PID controllers operate as one of the primary methods for robot motion control because they provide simple yet effective control solutions. The adaptive PID controller shows better stability performance along with rapid responsiveness during joint motion tracking operations applied Sliding Mode Control (SMC) for haptic robot trajectory tracking while showing its capability to resist dynamic disturbances[6].

The high-frequency control switching problem known as chattering in SMC systems becomes easier to handle through the implementation of higher-order SMC techniques. Fractional Order Control and Metaheuristic Optimization. The implementation of Fractional-Order PID (FO-PID) controllers as modern control methods represents an advancement over traditional PID controllers by offering better control flexibility. When using fractional calculus operators one can achieve better control parameter precision which results in enhanced system stability together with improved trajectory tracking capabilities, further applied two metaheuristic optimization methods PSO and GWO for FO-PID controller tuning toward a 3-Omni-Wheel Mobile Robot system. Research established that GWO-tuned FO-PID controllers demonstrated superior performance than conventional PID controllers regarding accuracy and response time as well as robustness[11].

1.4 Role of DC-DC Converters

DC-DC converters play a crucial role in modern power electronic systems by efficiently regulating and converting direct current (DC) voltage levels to meet the specific requirements of various applications. These converters are essential for ensuring optimal performance, energy efficiency, and stability in systems ranging from renewable energy sources like solar panels and fuel cells to electric vehicles, portable electronic devices, and industrial automation. By stepping up (boost) or stepping down (buck) the input voltage, or even providing isolated outputs, DC-DC converters enable seamless integration of diverse components with different voltage ratings. They also contribute to power quality improvement, protection against voltage fluctuations, and enhancement of battery life and system reliability.

1.5 Literature Review of DC-DC Converters

The rising need for more energy-efficient systems and the greater use of renewable energies have moved DC-DC converters into a leading position in modern power electronics. Because of these converters, the voltage levels between various sources and sensitive loads are kept in balance. Scholars have turned to standard PID controllers as well as advanced intelligent ones to handle fluctuating conditions in high-performance regulation. The tuning method sets the controller parameters as K_p, K_i, K_d using only the values of the passive components (R,L,C). MATLAB/Simulink simulations showed that the voltage regulator reaches a stable point rapidly and with higher than 99% accuracy for all load cases examined. Additionally, Susilo et al. [2] studied the behavior of a buck-boost converter controlled by PID techniques in Proteus simulation for solar PV systems. The technique allowed them to stabilize output voltage at around 24 V as input voltage changed from 12 V to 40 V, resulting in errors no higher than 5%. Their research found PID control is well suited to maintaining output stability in renewable energy systems. Testing found that PID controllers handled transient events better and responded more quickly than PI controllers, particularly in situations where load was not constant. It showed that adding a derivative element to the control loop helps dampen oscillations and improves how the system responds to changes in speed.

To counter the drawbacks of fixed-gain PID regulators, scholars have developed clever techniques such as fuzzy logic and neuro-fuzzy systems. Darvill et al. [4] have designed an ANFIS-PI controller for a boost converter supplied by a solar PV source. The ANFIS was trained with Particle Swarm Optimization (PSO) and adaptively tuned PI controller gains. This approach greatly enhanced voltage regulation, reduced deviation, and provided quicker transient response than traditional Fuzzy-PI control. DC-DC converters are critical components of renewable energy systems as they provide stable voltage outputs in the face of environmental and load variations. From the number of topologies available, the Single-Ended Primary Inductor Converter (SEPIC) is noteworthy for its potential to step up and step down the voltage while maintaining polarity. Its low input current ripple, non-stop input/output current supply, and minimized voltage stress enable it for photovoltaic (PV) and battery-based applications. Verma and Kumar [1] analyzed a SEPIC converter for PV applications using simulation and hardware experimentation. Their results indicated stable voltage and current at different solar irradiance employing Continuous Conduction Mode (CCM), which reduced voltage ripple and improved dynamic control. Their hardware realization included an Arduino-based gate driver and 10 kHz MOSFET switching stage at a 50% duty cycle [2].

Analytical analysis in [3] contrasted SEPIC performance in CISM-CCM, IISM-CCM, and IISM-DCM operation modes. CISM-CCM always yielded the lowest voltage ripple, with increasing ripple and switching stress under DCM. Careful inductor and capacitor selection optimized efficiency while reducing ripple.

Standard PI controllers underperform under nonlinear and time-varying conditions. In contrast to this, fuzzy logic controllers (FLCs) change the duty cycle with voltage error and rate of change of it, with improved response and higher stability. Elkhateb et al. [10] designed an FLC-based MPPT for SEPIC-PV systems through asymmetric membership functions, which yields a 4.8% power gain and 4.2% THD reduction. Ardhenta et al. [5] introduced a fuzzy-tuned PID controller in which fuzzy logic dynamically modifies PID gains in real time. This method enhanced the recovery time, overshoot reduction, and voltage stability under different conditions. More sophisticated techniques such as ANFIS [6] and Bat Algorithm-optimized PI [7] provide better adaptability and control. State-space modeling [8] and co-simulating tools such as MATLAB/Simulink and PSIM enhance accuracy and performance evaluation.

1.6 Outline of Dissertation

This dissertation is divided into different chapters. The summary of various chapters is given below:

Chapter 1 – In this chapter two systems are researched: 3-DOF haptic device and DC-DC converters (buck, boost, SEPIC) for renewable energy systems. A concise literature review describes used approaches and points out the research gaps covered in this thesis.

Chapter 2 – This chapter outlines the design and specifications of the 3-DOF haptic device. It describes the forward and inverse kinematics required for accurate end-effector motion and presents the path tracking and position control strategies used. Simulation results prove the efficacy of PI and PID controllers in providing accurate and stable operation of the device.

Chapter 3 – This chapter offers an overview of DC-DC converters—buck, boost, and SEPIC—highlighting their operating principles and real-world applications. It gives the mathematical modelling of all topology to study their dynamic behavior and control requirements. The discussion forms the basis for implementing and comparing different control strategies in later chapters.

Chapter 4 – In this chapter, control strategies like PID, Fuzzy Logic, and Adaptive Neuro-Fuzzy Inference System (ANFIS), are used for both haptic device and DC-DC converters are discussed. It describes the structure, tuning, and implementation procedures of each controller, highlighting their appropriateness for nonlinear and dynamic systems.

Chapter 5 – This chapter includes the final hardware setup of the robotic system, experimental results and a detailed discussion of the system's performance.

Chapter 6 – This chapter focuses on the simulation and analysis of DC-DC Converters & the output voltage waveforms obtained from the simulations.

Chapter 7 – This chapter introduces the hardware implementation of the buck converter circuit, highlighting the hardware configuration and gate triggering implementation with a 555 timer IC.

Chapter 8 – This chapter provides the key outcomes of the whole project and highlights the effectiveness of the proposed design and implementation. In addition, this chapter presents areas of future improvement.

CHAPTER 2

3 DOF ROBOTIC SYSTEM – STRUCTURE, OPERATION, AND KINEMATICS

2.1 OMNI Bundle

The rapid progress of robotics has necessitated agile, intelligent, and flexible systems. Omni-bundle robots, which merge omnidirectional mobility with modularity, are ideal for dynamic environments with high maneuverability and flexibility needs. Supporting omnidirectional wheels and modular modules, these robots can function individually or in conjunction with each other, and are best suited for warehousing, manufacturing, rescue, and service operations. Their modularity provides scalability, fault tolerance, and reconfigurability, improving operational performance. Central to their function is realistic kinematic and dynamic modeling, which allows for accurate motion planning and coordination. Their control strategies generally incorporate inverse kinematics, motion control algorithms, and sensor feedback, vision systems, or AI in real time.

The aim of this project is to design, model, and control an Omni-Bundle Robotic System to improve autonomous mobility and cooperative task performance, ranging from hardware design to kinematics, control design, and verification using simulation or experiments.



(a)



(b)

Fig 2.1(a) OMNI haptic device, (b) Board

2.2 System Specifications

The Omni Bundle is the first package of its kind to introduce robotics and haptics education using a friendly MATLAB/Simulink user interface. Bringing

together the QUARC software, a haptic device (previously called Sensable Phantom Omni) and the many Quanser developed curriculum tools enables students to transition from learning theory to practical use.



Fig.2.2 Links L_1, L_2, L_3 of omni device

Three of the six revolute joints in the Geomagic Touch haptic device are actuated. The wrist joints comprise the group of three non-actuated joints. Together, the three drivers are able to move the end-effector across all directions in the robot's workspace. Rotational movement along roll, pitch and yaw is detected by potentiometers, while all other position measurements are done with digital encoders. The Phantom Blockset gives a clear way to interface with QUARC real-time control software.

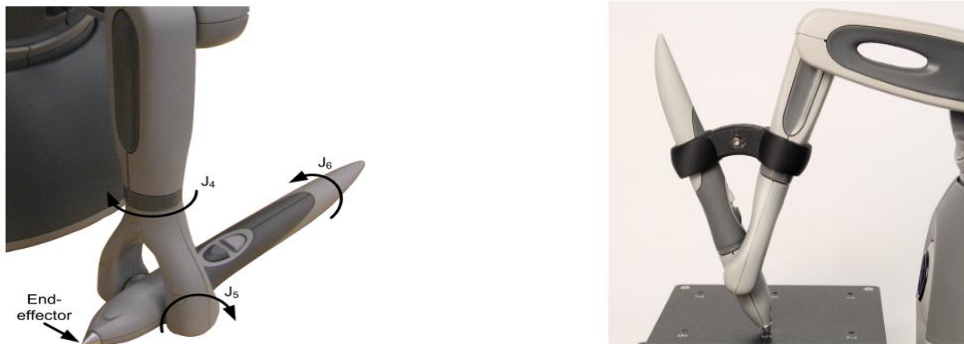


Fig.2.3 stylus of robot

Table 2.1 system specifications of device

PARAMETER	VALUES
workspace (W x H x D)	160 mm x 120 mm x 70 mm
Footprint (physical area the device occupies on desk)	168 mm x 203 mm
Device mass	1.8 Kg
Stiffness	1.26 N/mm (x axis) / 2.31 N/mm (y axis) / 1.02 N/mm (z axis)
Maximum force	3.3 N
Interface	Ethernet
DC servo motor	6 volts

2.3 Robotic Kinematics

Any robotic manipulator is designed to perform a specific task in the 3D space. This requires control of each link's position and the manipulator's joint to control the tool position and orientation. Due to the highly non-linear nature of the system, a mathematical model of the device is required to control the tool and joint link motions, in that way, kinematics dynamics play an important role.

2.3.1. Forward Kinematics (FK)

FK means finding out the end-effector's position and orientation from the known joint parameters in robotics.. It plays a crucial role in determining how individual joint movements translate into motion in space, allowing engineers and roboticists to predict the spatial configuration of the robot's tool or gripper. For instance, in a robotic manipulator with revolute and prismatic joints, forward kinematics calculates the final pose of the end-effector using the angles or displacements of each joint. This process is typically implemented using transformation matrices that describe the rotation and translation between successive links. In more complex systems, the Denavit-Hartenberg (DH) convention is widely used to systematically model each link and joint through a set of four parameters, leading to the construction of homogeneous transformation matrices. By multiplying these matrices sequentially, one can determine the complete transformation from the robot's base frame to its end-effector. Forward kinematics is essential for tasks such as path planning, simulation, and motion control, forming the basis for trajectory generation and enabling the integration of sensor feedback in intelligent robotic systems.

Table 2.2 D-H parameter

$\Theta(\text{rad})$	$d(\text{m})$	$a(\text{m})$	$\alpha(\text{rad})$
q1	0	0	$-\pi/2$
q2	0	L_1	0
q3	0	L_2	0

When the Denavit-Hartenberg convention is used on the manipulator, the transformation matrix is obtained. Link length - a_i , Link twist - α_i , Joint distance - d_i and Joint angle - θ_i are known as the D-H parameters.

$$R_{x,\alpha} = \begin{bmatrix} \cos \theta & -\sin \theta & 0 & 0 \\ \sin \theta & \cos \theta & 0 & 0 \\ 0 & 0 & 1 & 0 \\ 0 & 0 & 0 & 1 \end{bmatrix} \quad T_{x,a} = \begin{bmatrix} 1 & 0 & 0 & a \\ 0 & 1 & 0 & 0 \\ 0 & 0 & 1 & 0 \\ 0 & 0 & 0 & 1 \end{bmatrix} \quad T_{x,d} = \begin{bmatrix} 1 & 0 & 0 & 0 \\ 0 & 1 & 0 & 0 \\ 0 & 0 & 1 & d \\ 0 & 0 & 0 & 1 \end{bmatrix} \quad R_{x,\alpha} = \begin{bmatrix} 1 & 0 & 0 & 0 \\ 0 & \cos \alpha & -\sin \alpha & 0 \\ 0 & \sin \alpha & \cos \alpha & 0 \\ 0 & 0 & 0 & 1 \end{bmatrix}$$

$$A1 = \begin{bmatrix} \cos(\theta_2) & -\sin(\theta_2) & 0 & L_1 \cos(\theta_2) \\ \sin(\theta_2) & \cos(\theta_2) & -1 & L_1 \sin(\theta_2) \\ 0 & 0 & 0 & 0 \\ 0 & 0 & 0 & 1 \end{bmatrix}, \quad A2 = \begin{bmatrix} \cos(\theta_1) & 0 & -\sin(\theta_1) & 0 \\ \sin(\theta_1) & 0 & \cos(\theta_1) & 0 \\ 0 & -1 & 0 & 0 \\ 0 & 0 & 0 & 1 \end{bmatrix},$$

$$A3 = \begin{bmatrix} \cos(\theta_3 - \frac{\pi}{2}) & -\sin(\theta_3 - \frac{\pi}{2}) & 0 & L_2 \cos(\theta_3 - \frac{\pi}{2}) \\ \sin(\theta_3 - \frac{\pi}{2}) & \cos(\theta_3 - \frac{\pi}{2}) & -1 & L_2 \sin(\theta_3 - \frac{\pi}{2}) \\ 0 & 0 & 0 & 1 \\ 0 & 0 & 0 & 1 \end{bmatrix}$$

Rotation matrix,

$$O = \begin{bmatrix} c_1 c_2 c_3 - s_1 s_2 s_3 & -c_1 c_2 s_3 - c_1 s_2 c_3 & c_1 s_2 - s_1 \\ s_1 c_2 c_3 - s_1 s_2 s_3 & -s_1 c_2 s_3 - s_1 s_2 c_3 & s_1 s_2 \\ -s_2 c_3 - c_2 s_3 & s_2 s_3 - c_2 c_3 & c_2 + 1 \end{bmatrix}$$

Position equations are-

$$x = L_1 \cos(\theta_1) \cos(\theta_2) + L_2 \cos(\theta_1) \cos(\theta_2) \cos(\theta_3 - \pi^2) - L_2 \cos(\theta_1) \sin(\theta_2) \sin(\theta_3 - \pi^2) \dots (2.1)$$

$$y = L_1 \sin(\theta_1) \cos(\theta_2) + L_2 \sin(\theta_1) \cos(\theta_2) \cos(\theta_3 - \pi^2) - L_2 \sin(\theta_1) \sin(\theta_2) \sin(\theta_3 - \pi^2) \dots (2.2)$$

$$z = L_1 \sin(\theta_2) - L_2 \sin(\theta_2) \cos(\theta_3 - \pi^2) - L_2 \cos(\theta_2) \sin(\theta_3 - \pi^2) \dots (2.3)$$

2.3.2. Inverse Kinematics (IK)

Inverse kinematics is used in both robotics and motion control for finding the necessary joint parameters to make a robotic manipulator reach a target position and/or orientation. Inverse kinematics is used to determine what joint angles that are required to move end-effector to the desired posture in space. Unlike forward kinematics, this method is complex enough that it may require solving nonlinear equations, attempting to find multiple solutions and checking that the answer is physically realistic, avoiding joint limits and singular problems. In order to handle tasks like object control, path planning and user interactions with precision, we use inverse kinematics in devices such as robotic arms and haptic interfaces.

$$\theta_1 = \tan^{-1}(y/x) \quad (2.4)$$

$$\theta_2 = \varphi - \gamma \quad (2.5)$$

$$\theta_3 = 3\pi/2 - \cos^{-1}(L_1^2 + L_2^2 - k^2 / 2L_1L_2) \quad (2.6)$$

$$k = \sqrt{X^2 + Y^2 + Z^2} \quad (2.7)$$

$$d = \sqrt{X^2 + Y^2} \quad (2.8)$$

$$\varphi = \cos^{-1}(d/k) \quad (2.9)$$

$$\gamma = \sin^{-1}(L_2 \sin(3\pi/2 - \theta_3) / k) \quad (2.10)$$

Where $L_1=L_2=0.132\text{m}$ represents link lengths, contributes in path planning/tracking with haptic guidance purposes

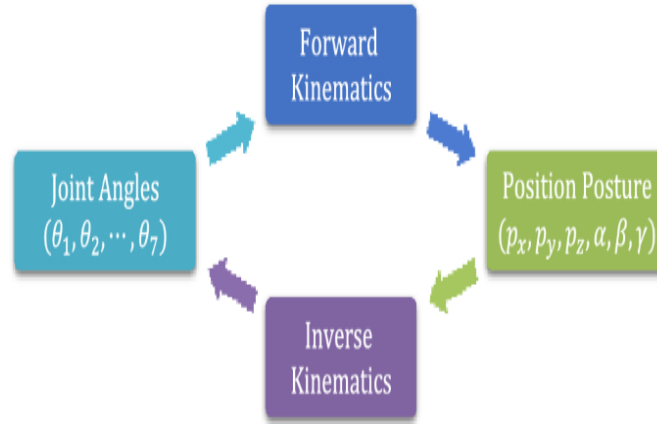


Fig 2.4 Block diagram of FK & IK kinematics

2.4 Position Control and Path Tracking

Controlling position in omni haptic devices is vital for precise and fast movement along the six available axes. Medical simulation, virtual reality and teleoperation often count on these devices for their accuracy. Going forward, programmers should concentrate on positioning the end-effector by reading user input or going down a planned path which will make the device give realistic touches. Joint movements are modeled using forward and inverse kinematics to find the displacement of the end-effector. Optimization of error in tracking is achieved by using PI, PID and model-based control algorithms.

During path tracking, the controller is fed updated position information from the system and uses encoders as feedback sensors to see where the vehicle really is. Based on a control algorithm, the robot adaptively changes actuator inputs to eliminate deviations and make its movements smooth in the face of disturbances from the outside. Because of this, the forces felt by players are steady and fairly realistic. In this project, specific positions for each joint are designed and analyzed by using PD controllers set with suitable gains to achieve the required goals. The model is simplified and the closed-loop diagram (Fig 2.3) illustrates how feedback is processed by the PV controller which improves the ability to track and the behavior as a second-order system.[5].

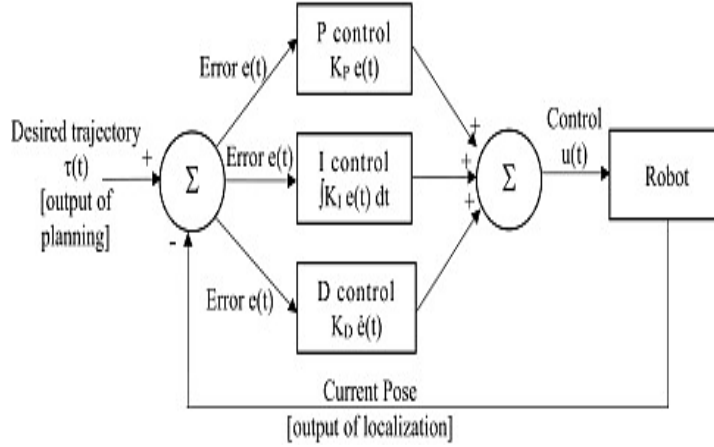


Fig. 2.5 closed loop control of PID controller

$$y(t) = K_{p(t)} \cdot e(t) + K_{d(t)} \cdot \dot{e}(t) + K_i \cdot \int e(t), dt \quad (2.11)$$

PD controllers may not fully eliminate steady-state error, especially in the presence of constant disturbances or modelling inaccuracies. To address this limitation, an integral term is introduced, resulting in a Proportional-Integral-Derivative (PID) controller. It gathers all the errors in position over the time and changes when the control is applied., thereby eliminating steady-state errors. In this work, both PD and PID controllers were tested for each joint to compare their performance under various conditions. Figure 3 presents the closedloop block diagram for the joint control architecture. The model used for controller design simplifies the joint dynamics by neglecting high-frequency nonlinearities such as

friction, backlash, and structural flexibility, enabling an initial focus on core controller performance.

It is also worth noting that in this implementation, the derivative action is applied directly to the measured position (velocity feedback), a method often referred to as PV (Proportional-Velocity) control. This contrasts with the traditional PD implementation where the derivative acts on the error signal. PV control improves damping characteristics and aligns the system's response more closely with that of a critically damped second-order system, providing better trajectory tracking with reduced sensitivity to noise in the error signal.

2.5 Applications of the OMNI Haptic Device

- **Medical and Surgical Simulation-** Used in virtual surgical training simulators for procedures such as laparoscopic surgery, dental surgery, or orthopedic tasks. Enables tactile feedback to simulate interaction with soft tissues, bones, and instruments.
- **Robotics and Teleoperation-** Acts as a master device in bilateral teleoperation systems for remotely controlling robotic arms with force feedback. Widely used in space robotics, underwater exploration, and minimally invasive surgery.
- **CAD and 3D Modelling-** Allows designers to “feel” and manipulate virtual 3D objects, enhancing precision and intuition in design.

2.6 Advantages of the OMNI Haptic Device

- **High Precision and Sensitivity-** Accurate position sensing and responsive force feedback suitable for fine motor tasks.
- **Compact and Lightweight Design-** Portable, desktop-friendly design makes it easy to integrate into lab setups or simulation platforms.
- **Real-Time Force Feedback-** Delivers immediate tactile responses, enhancing realism and immersion in interactive simulations.

2.7 Conclusions

This chapter presents a detailed exploration of the design, modelling, and control of a 3-Degree-of-Freedom (3-DOF) haptic device. It begins by outlining the specifications and structural design, describing the mechanical components such as joints, links, actuators, and sensors that form the physical architecture of the device. The mechanical design emphasizes modularity, precision, and ease of integration into applications such as surgical simulators, virtual environments, and remote manipulation systems. A significant portion of the chapter is devoted to the mathematical modelling of the device, specifically addressing forward and inverse kinematics. Path tracking and position control strategies are introduced to ensure the haptic device follows predefined trajectories with minimal error. The implementation of classical PI and PID controllers is described to achieve desired performance in terms of responsiveness, stability, and accuracy.

CHAPTER 3

DC-DC CONVERTERS – OPERATION, MODELLING AND APPLICATION

3.1 DC-DC Converters

A converter is an electrical circuit that takes DC input voltage and generates a different level of DC voltage, usually employing high-frequency switching and inductive-capacitive filters. It alters electrical energy for particular applications—increasing voltage, changing polarity, or generating multiple outputs with changing signs. There are six primary classes of converters: AC to DC, DC to DC, AC to AC, DC to AC, and Static Switches. Converters include two major parts: controllers and filters. Filters drive the electrical signals, and their construction in many cases is based on the Maximum Power Transfer Theorem. Controllers play the role of the system's mind, deciding how the converter (the heart of the system) works. Together, they control power flow and guarantee energy conversion efficiency. Converter design includes both power and control circuitry. They are crucial in systems that need stable and precise power, such as renewable energy configurations, electric vehicles, portable devices, and industrial automation. Converter circuits convert direct current from a power source to a desired voltage level, making energy use reliable and flexible in most modern applications.

TYPES OF DC-DC CONVERTERS

1. **Buck Converter (StepDown)**

Reduces the input voltage to lower output voltage. Used where a lower voltage is required than the supply.

$$V_{out} = D \cdot V_{in} \text{ , where } D \text{ is the duty cycle.}$$

2. **Boost Converter (StepUp)**

Increases the input voltage to higher output voltage. Common in battery-powered systems needing higher voltage.

$$V_{out} = \frac{1}{1-D} V_{in}$$

3. **SEPIC Converters**

Provide non-inverted output voltage with the ability to stepup or stepdown. They offer smoother input and output current.

3.2 Buck Converter

A Buck Converter is a DC-DC converter that steps down a higher input voltage to a lower output voltage and has high efficiency. It works on the operation of a switching element (most commonly a MOSFET or transistor), a diode, an inductor, and a capacitor.

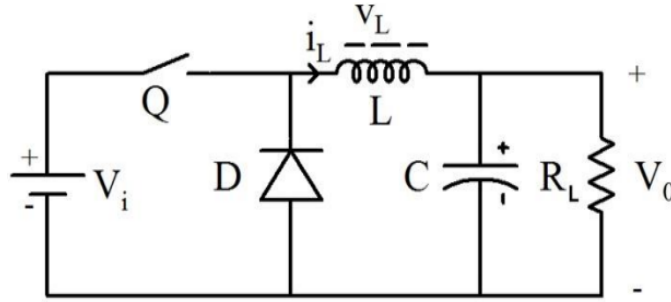


Fig 3.1 Basic buck converter circuit

The Buck Converter operates in two main modes during each switching cycle:

1. On-State

The inductor stores energy and the capacitor stores its charge. The voltage on the capacitor will be seen across the load. By using KVL, the voltage across the inductor comes out as the difference of the supply voltage (V_S) and the output voltage (V_O).

$$V_L = V_S - V_O \quad (3.1)$$

$$\frac{di_L}{dt} = \frac{V_S - V_O}{L} \quad (3.2)$$

$$L \frac{di_L}{dt} = V_S - V_O \quad (3.3)$$

$$D = T_{ON}/T \text{ (where } T = T_{ON} + \text{OFF)}$$

During the ON period of the switch, $T_{ON} = DT$ thus $\Delta t = DT$. Therefore, the above equation can be written as,

$$\frac{\Delta i_L}{\Delta t} = \frac{V_S - V_O}{L} \quad (3.4)$$

$$\frac{\Delta i_L}{DT} = \frac{V_S - V_O}{L} \quad (3.5)$$

$$\Delta i_L = \left(\frac{V_s - V_o}{L} \right) DT \quad (3.6)$$

2. When Switch is OFF

With mode-II, the inductor acts as the power supply when the switch opens and cuts off power to the load. Because the inductor polarity changes during this phase, the diode now gets forward-biased. Thus, the inductor's current flows through the capacitor, load and diode as highlighted below.

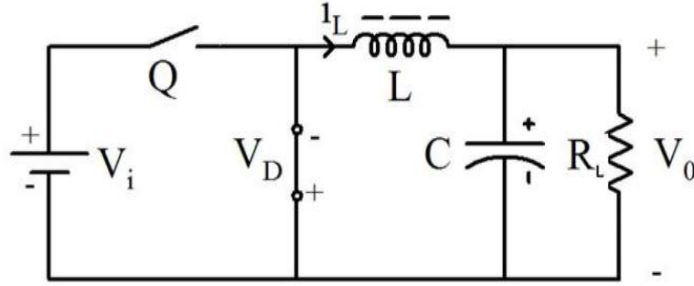


Fig 3.2 off mode operation

The flow of current will keep going through the load until the current in the inductor drops to zero value. When the inductor is fully discharged, the diode becomes reverse biased and the switch is again closed thus repeating the cycle.

$$\begin{aligned} 0 &= V_L + V_o \\ V_L &= L \, di_L/dt = -V_o \\ T &= T_{ON} + T_{OFF} \\ T &= DT + T_{OFF} \\ T_{OFF} &= (1 - D)T \\ T_{OFF} = \Delta t &= (1 - D)T \end{aligned}$$

Substituting above Δt in equation we get,

$$L \frac{di_L}{dt} = -V_o \quad (3.7)$$

$$L \frac{\Delta i_L}{(1 - D)T} = -V_o \quad (3.8)$$

$$\Delta i_L = -\frac{V_o}{L} (1 - D)T \quad (3.9)$$

$$\Delta i_L^{(closed)} + \Delta i_L^{(open)} = 0 \quad (3.10)$$

$$\frac{V_s - V_o}{L} DT + \left(-\frac{V_o}{L} (1 - D)T \right) = 0 \quad (3.11)$$

$$\frac{V_o}{V_s} = D \quad (3.12)$$

The above equation provides the rate of change of current through the inductor when the switch is closed. The net change of current through the inductor for one supply cycle will be zero.

If assume the switch is turned on again before the inductor current goes to zero then a continuous load current operation is achieved. If the switch is turned on after the complete discharge of the inductor then the load current will be discontinuous. By adjusting the switching frequency, the voltage regulation is regulated. If TOFF is increased the average output voltage is decreased, if TOFF is reduced, the average output voltage is increased.

Operating Modes of Buck Converter

Continuous Conduction Mode (CCM) and Discontinuous Conduction Mode (DCM) are the two main modes of a Buck Converter, which are determined by the behaviour of the inductor current during a single switching cycle. 1. CCM, or continuous conduction mode Throughout the whole switching cycle (including ON and OFF periods), the inductor current in CCM never drops to zero.

- The energy stored in the inductor is always partially maintained. The inductor current has a ripple but remains positive. This mode is typically



Fig 3.3(a) CCM

desired in high-load conditions for smoother output and better efficiency. Output voltage:

$$V_{out} = D \times V_{in}$$

Inductor current ripple:

$$\Delta I_L = (V_{in} - V_{out}) \times D \times T_s / L$$

2. Discontinuous Conduction Mode (DCM)

In DCM, the inductor current falls to zero for a portion of the switching cycle.

- Occurs at light-load conditions when the inductor cannot sustain continuous current. In each cycle, the inductor current rises, falls to zero, and stays at zero for a part of the period. More complex to control and analyze due to dependence on load current. The output voltage is no longer linearly proportional to the duty cycle.



Fig 3.3(b) DCM

Table 3.1 Comparison

Feature	CCM	DCM
Inductor current	Always > 0	Drops to 0 during cycle
Output voltage	Linear with duty cycle	Nonlinear with duty cycle
Control complexity	Simpler	More complex
Efficiency (light load)	Lower than DCM	May be better at very light loads
Ripple current	Lower	Higher

3.3 Boost Converter

A boost converter, or step-up DC-DC converter, boosts the input voltage to a greater output voltage. It is a voltage regulator, giving output that is equal to or greater than the input. In most industrial and domestic applications, the ability to convert a fixed DC voltage to an adjustable level is needed. A DC chopper does just this, as a transformer does for AC, facilitating step-up or step-down voltage conversion. DC choppers have some advantageous properties, such as high efficiency, quick response, compact size, smooth and easy control, low maintenance, and cost-effectiveness, which make them very suitable for various power regulation applications.

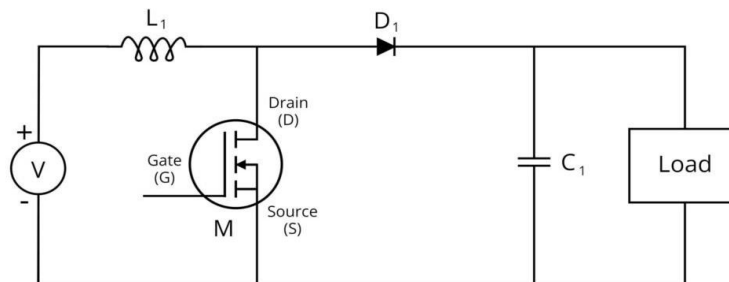


Fig.3.4 basic boost converter circuit

A diode is connected in series with the load after the power MOSFET which also acts as the switch by automatically forward biasing and reverse biasing. A

capacitor in parallel is placed at the load side for removing ripples in the output signal.

The high-speed ON/OFF semiconductor switch (power MOSFET) will alternatively connect and disconnect the load from the supply at a rapid rate so that a voltage of higher magnitude than the input voltage will appear at the output side. The semiconductor switch (power MOSFET) is turned ON and OFF by controlling the gate terminal using Pulse Width Modulation(PWM).

Working of Boost Converter

With the use of a boost converter, we can generate an output signal of more than the input signal. First, the power MOSFET is switched ON by giving a signal at gate terminal. Now the supply current (I_{in}) begins to flow through the inductor (L) and power MOSFET as indicated below.

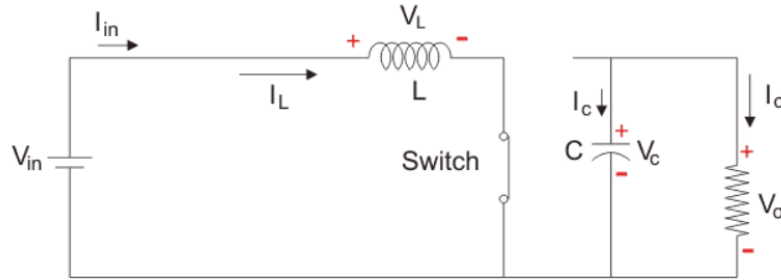


Fig 3.5 boost when switch is open

The inductor current (I_L), which is charged with a polarity according to the direction of supply current flow as mentioned above, starts to increase once the power MOSFET is turned on. From the minimum to the maximum, the inductor current rises linearly. Because of the energy stored in the capacitor, which is visible across the cathode (the anode is at zero volts due to the conducting power MOSFET), the diode is reverse biased. Thus, the load from the supply will be switched off by the reverse biased diode. The capacitor supplies a steady load current if the capacitance is quite high. Now that the power MOSFET is off, the inductor is receiving supply current.

$$V_L - V_o + V_{in} = 0$$

$$V_L = V_o - V_{in}$$

During TOFF time of mosfet , V_o will be attributed to the supply and inductor. As soon as switch is OFF, I_L will begin decreasing to I_{min} , and I_D will equal I_L . By applying KVL to the circuit when MOSFET is OFF, we will obtain

The energy supplied to the inductor during the ON period of switch is given as,

$$W_{ON} = \text{Voltage across the inductor} \times \text{Average current through inductor} \times T_{ON}$$

$$W_{ON} = V_{in} (i_{min} + i_{max}/2) T_{ON}$$

Also, the energy supplied by the inductor during the OFF period of MOSFET is given

$$W_{OFF} = \text{Voltage across the inductor} \times \text{Average current through inductor} \times T_{OFF}$$

$$W_{OFF} = V_o - V_{in} (i_{min} + i_{max}/2) T_{OFF} \quad (3.13)$$

$$V_o \cdot T_{OFF} = V_{in} \cdot T \quad (3.14)$$

$$V_o = V_{in} \cdot \frac{T}{T_{OFF}} \quad (3.15)$$

$$V_o = V_{in} \cdot \frac{T}{T - T_{ON}} \quad (3.16)$$

$$V_o = V_{in} \cdot \frac{1}{\left(\frac{T}{T} - \frac{T_{ON}}{T}\right)} \quad (3.17)$$

We know that duty cycle $\alpha = \frac{T_{ON}}{T}$

$$V_o = V_{in} \cdot \frac{1}{1 - \alpha} \quad (3.18)$$

The duty ratio affects how much voltage you will get from the converter. From $\alpha = 0$ to $\alpha = 1$, the output of the circuit is greater than the input, so the voltage is increased.

3.4 SEPIC Converter

The SEPIC converter circuit is shown in Fig.3.6 shows that the circuit of SEPIC converter consists of coupling capacitor C1, output capacitor C2, two inductors L1, L2, diode D and Power mosfet as switch S1. Assuming CCM the, various modes of operations are discussed below when switch is ON and when the switch is off.

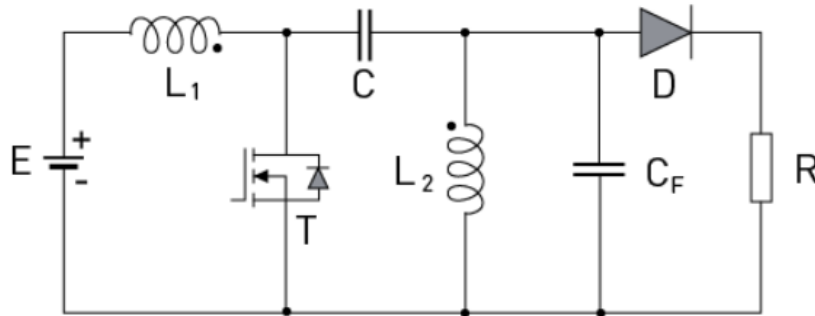


Fig 3.6 SEPIC converter circuit

A) Basic working of SEPIC: Mode I: ($0 < t < DT_s$)

When switch S is switched ON, inductor L1 starts to charge from source voltage V_s and stores energy in its magnetic field. Meanwhile, it is considered that the coupling capacitor C_p has already been pre-charged up to the input voltage V_{in} . When S is switched ON, C_p starts discharging through secondary inductor L2, thereby providing a current path. As per the polarity indicated in Fig.2(a), the diode's orientation causes it to be reverse-biased throughout

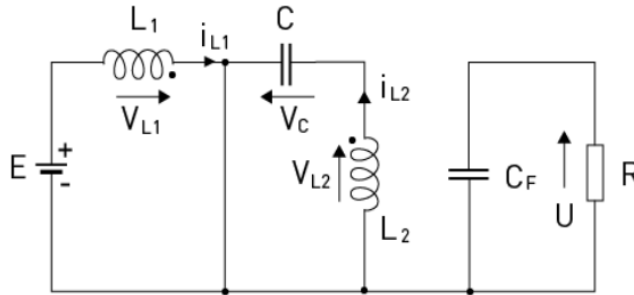


Fig.3.7(a) Mode 1 circuit Operation

this period. Due to the reverse bias, the diode prevents current from flowing into the output stage and hence does not allow the output capacitor to receive any charge at this time. In essence, in the switch ON state, energy is charged in L1, and C_p delivers energy across L2 without adding to the output. The phase is responsible for setting up the circuit to the next level of the energy transfer process.

B) Mode II: ($DT_s < t < T_s$)

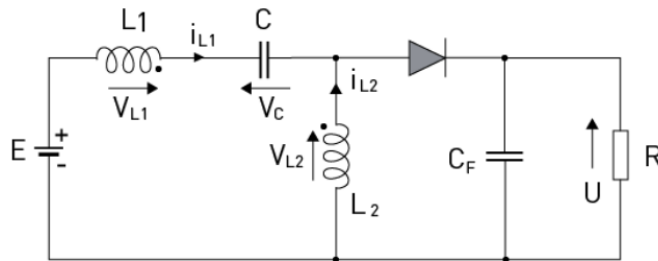


Fig.3.7(b). Mode 2 operation

When switch S is turned OFF, the SEPIC converter transitions into its OFF-state operation, as shown in Fig.2(b). In this mode, inductor L1, which had been storing energy during the ON-state, begins to discharge through the coupling capacitor C_p , thereby transferring energy and charging it. Meanwhile, inductor L2 reacts to the sudden change in the current by reversing its polarity, as dictated by Lenz's Law. This reversal forward-biases diode allowing it to conduct. Consequently, L2

discharges its energy through output capacitor and load, ensuring continuous power delivery during the switch OFF interval. The charging of C_p prepares it to release energy in the next cycle when the switch turns ON again. This energy transfer process ensures voltage regulation and continuous output, even under dynamic load and input conditions, making SEPIC converters highly reliable for power-sensitive applications[12].

$$V_{L1} = -E \quad (3.19)$$

$$V_{L2} = -V_C = -E \quad (3.20)$$

$$V_{L2} = U \quad (3.21)$$

$$V_{L1} = U + V_C - E = U \quad (3.22)$$

$$E \cdot T \cdot d = U \cdot T \cdot (1 - d) \quad (3.23)$$

$$U = E \cdot \frac{d}{1 - d} \quad (3.24)$$

$$D = \frac{V_{out}}{V_{in} + V_{out}} \quad (3.25)$$

$$V_{out} = V_{in} \cdot \frac{d}{1 - d} \quad (3.26)$$

$$V_{out} \cdot (1 - d) = V_{in} \cdot d \quad (3.27)$$

$$V_{out} \cdot V_{out} \cdot d = V_{in} \cdot d \quad (3.28)$$

$$d = \frac{V_{out}}{V_{in} + V_{out}} \quad (3.29)$$

Buck converter applications (step-down):

1. PC and server motherboards: 12 V \rightarrow 5 V/3.3 V/1 V core rails
2. Phone / tablet PMICs: 4 V battery \rightarrow 1.8 V, 1.2 V logic supplies
3. DC motor speed control when the supply voltage is already higher than needed

Boost converter applications (step-up):

1. Power banks: single-cell Li-ion (2.5–4.2 V) \rightarrow regulated 5 V USB-A/C port
2. Portable white-LED flashlights and LCD backlights (3 V cell \rightarrow 9–12 V LED string)

SEPIC converter applications

1. Automotive USB-C/fast-charge adapters: 7–16 V car battery \rightarrow fixed 5 V or 9 V
2. Hand-held devices that run on battery **and** wall adapter (3–15 V in) but require a constant 5 V logic rail

ADVANTAGES

Buck (step-down)

1. Highest efficiency of any non-isolated topology (often > 95 %), so it stays cool and extends battery life.
2. Simplest, lowest-cost part count—just one inductor, switch, diode, and capacitor—making layout and EMI control straightforward.

Boost (step-up)

1. Lets low-voltage sources (e.g., single-cell Li-ion) drive higher-voltage loads in a single stage, avoiding extra batteries.
2. Draws a continuous input current, which reduces conducted EMI and eases input-filter sizing.

SEPIC (buck-or-boost, same polarity)

1. Delivers a fixed, positive output whether the input falls below, equals, or exceeds it—ideal for wide or unpredictable supplies.
2. Maintains continuous input current like a boost, keeping electromagnetic emissions low while avoiding the polarity inversion of a classic buck-boost.

3.5 Conclusions

This chapter provides an analysis of DC-DC converters—buck, boost, and SEPIC focusing on their operating principles and practical applications in renewable energy systems. It presents the mathematical modelling of each topology to analyse their dynamic behavior and control requirements. The discussion sets the foundation for implementing and comparing various control strategies in subsequent chapters.

CHAPTER 4

CONTROL METHODOLOGIES

4.1 Open Loop VS Close Loop

Control System is a system where the system's behavior is governed by a differential equation. It regulates the devices and the systems through control loops. There is Open-Loop Control System and Closed-Loop Control System. Open-Loop Control System is used where feedback and error correction is not necessary.

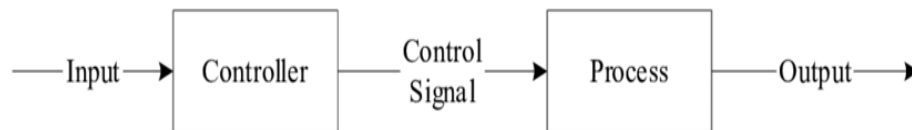


Fig.4.1 open loop

ClosedLoop Control System is used in the applications where feedback and error handling are required. It is a very complex system and not economical but optimization is possible.

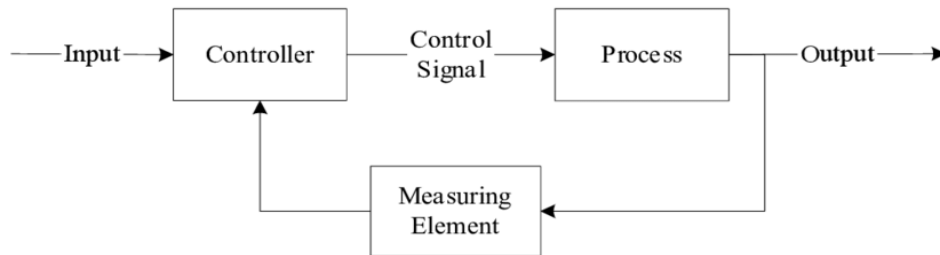


Fig.4.2 closed loop with a feedback

4.2 Types of Controllers

There are four control types in the PID controller family and they are called the proportional (P), proportional plus integral (PI), proportional plus derivative (PD) and proportional plus integral plus derivative (PID) controllers.

4.3 Classical PID Controller

The PID controller is the most common control form used in industrial processes, which incorporates proportional (P), integral (I), and derivative (D) actions. Developing from Minorsky's 1922 research in automatic steering stability, the PID controllers have been used for almost a century in linear and nonlinear processes. They can be employed singly (P, I, or D) or in pairs as PI, PD, or PID to generate control signals that drive systems toward stability and reduce errors. Even with improvements in intelligent control, PID controllers are still essential components of approximately 95% of contemporary industrial closed-loop systems because they are simple and effective.

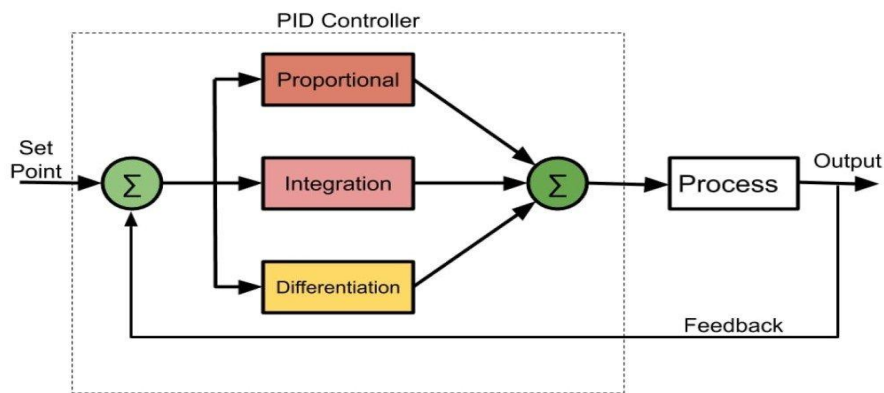


Fig.4.3 Block diagram of PID controller

Advantages of PID controller

- 1) PID controller are simple, efficient. They offer fast response, stability and adaptability.

Disadvantage

- 1) This controller may struggle in complex linear system
- 2) Optimal tuning can be challenging due to the (P, I and D) parameters

4.4 Fuzzy Logic Control System (FLC)

Fuzzy Logic Control (FLC) is a control method that boosts industry, medical device, financial and security control systems using fuzzy theory. FLC performs well on difficult, cloudy problems even without knowing the system in great detail. Control systems are built using physical devices that change the behavior of an other system. There are basically two categories of feedback systems: open-loop and closed-loop. In contrast to their open-loop system counterparts, closed-loop systems use measured results to update or modify what they are doing. The process

being controlled has sensors that measure its variable and the system is the plant. The control system adjusts itself by using the difference between the desired result and the actual result. Controllers and compensators increase the performance of a system by reducing the number of errors. Using IF-THEN rules in fuzzy control is an efficient method to control difficult systems.

ARCHITECTURE AND OPERATIONS OF FLC SYSTEM

Fig. 4.4 shows what parts a fuzzy logic controller consists of. Those components are fuzzifiers, fuzzy rule bases, fuzzy knowledge bases, inference engines and defuzzifiers in an FLC system. We observe that the models include parameters for normalising signals. The system uses fuzzy logic to decide what action to take when the defuzzifier does not give a command. It means the fuzzifier changes exact values into values that are less exact. Efficiency specialties use fuzzy rules to summarize their knowledge about the process. All the fuzzy relationships between input and output are saved in a fuzzy knowledge base. The membership functions assign values to each input variable in the fuzzy rule base and the output value of the plant being controlled. The inference engine lies at the heart of an FLC system and can imitate how humans take decisions to reach the right control strategy. From the fuzzy action recommended by the inference engine, the defuzzifier creates clear and simple instructions.

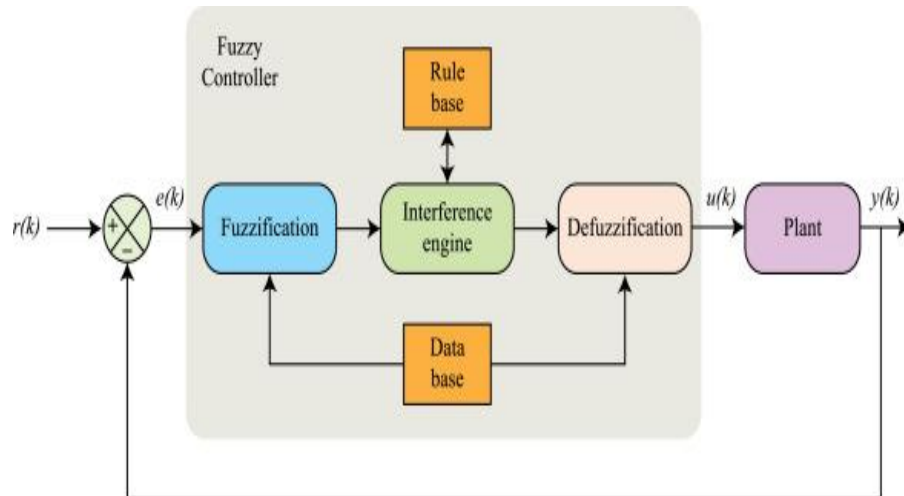


Fig 4.4 Basic architecture of FLC System

4.5 ANFIS

In ANFIS, the parameters of membership functions that are optimized through hybrid learning to minimize the difference between the predicted and actual values. Careful tuning of the number of training epochs, the type and number of membership functions, and the complexity of the fuzzy rules is essential to avoid underfitting or overfitting the model. By combining the interpretability of fuzzy logic with the learning capability of neural networks, ANFIS can efficiently manage systems with multiple inputs and a single output. This makes it highly effective for the modeling and control of complex, nonlinear systems.

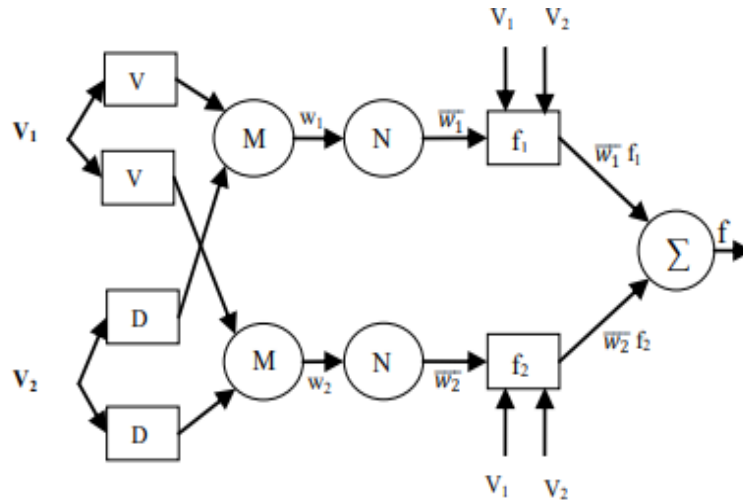


Fig 4.5 Adaptive neuro architecture

4.6 Layers of ANFIS

This discussion considers the fuzzy inference system having just two inputs, v and d and one output, f . I have included a brief explanation of five steps in the ANFIS algorithm.

Layer 1

In this input layer, each node i is flexible and creates a membership grade for a linguistic label. It is a soft boundary, where v and d are supplied from the surroundings.

Layer 2

The second layer weighs each membership function, accepts data from the first layer and serves as a representation for fuzzy sets of specific input values.

Here, all nodes at this layer are anchored and each carries the M label; the output results from every signal being productively summed.

Layer 3

Each node in this layer is set at the middle, with a circle labeled N, demonstrating that it gets normalized to the strength of the previous layer's signals. Pre-condition matching on fuzzy rules is done by this layer and the number of layers is the same as the number of fuzzy rules.

Layer 4

By using the designated function, this layer gives output values y after applying the rules. The result comes from applying the normalized firing rule strength to a first order polynomial. The impact of a rule is shown by the weight of the node in the network.

Layer 5

All the information coming from layer 4 is added in the output layer and is then converted into usable values.

4.7 Learning Algorithm of ANFIS

With neuro-adaptive learning, the fuzzy modelling method now has the ability to recognize patterns in the data. It looks for the best membership function parameters to support the fuzzy inference system in tracking the input/output examples. These parameters in the membership functions are altered during learning [19]. To address real-world issues more efficiently, the job of this architecture's learning algorithm is to optimize all tweakable settings and have the output of ANFIS fit the training data. If we want to get the network to converge faster, we can make it learn using a hybrid algorithm that uses both the least square method and gradient descent. To find the optimal outcomes for layer 4, we can apply the least squares method when using fixed premise parameters on the earlier layers. Gradient vector indicates the quality of modeling input/output data by the fuzzy inference system using a group of parameters. Any of several optimization strategies can be used to fix the parameters so that the error measure drops when the gradient vector is identified [19]. If the training parameters are not set in advance, then the training takes longer to finish. The hybrid algorithm has a forward phase which uses the LSM and a backward phase which uses the GDM. When the convergence criteria are met for consequent parameters, the computation process proceeds in a backward manner. During the backward pass, errors are moved backwards and the parameters of the rule for the fuzzy sets in the input area are adjusted with the gradient descent method [11]. A combination of least squares estimation and back-propagation is used by ANFIS to determine the values of its membership functions.

Applications

Renewable Energy: To control solar inverters or wind turbines.

Robotics: For smooth and adaptive motion control.

Power Electronics: To manage voltage and current in converters.

Forecasting: Like predicting weather, load, or energy demand.

4.8 Conclusions

This chapter explores various control strategies including PID, Fuzzy Logic, and Adaptive Neuro-Fuzzy Inference System (ANFIS) applied to the haptic device and DC-DC converters. It explains the structure, tuning, and implementation methods for each controller, emphasizing their suitability for nonlinear and dynamic systems. The chapter also outlines the ANFIS architecture, highlighting its learning capability and adaptability in complex control scenarios.

Chapter 5

HARDWARE RESULTS OF ROBOTIC SYSTEM

5.1 Robotic System

Modelling of the kinematics and dynamics of a haptic system (3-DOF devices).Design and test control algorithms (e.g.position control, force feedback).Evaluate user interaction fidelity through simulation before physical prototyping. Integrate real-time feedback loops with external hardware (via Simulink Real-Time).

Tools Used -Simulink Control Design PID/State feedback tuning, system linearization.

5.2 Forward and Inverse Kinematics Analysis

Table 5.1End Effector Position With Forward Kinematics Analysis

Position	Joint Angles	Tool position	End effector position		
Pos 1	0.6254	0.1176	0.1397	-0.7986	0.5854
	-0.264	0.08617	0.1009	0.5767	0.8107
	3.232	0.05684	0.985	0.1723	$6.123e^{-17}$
Pos 2	0.01645	0.1176	0.01874	-0.997	0.0164
	-0.2607	0.08617	0.00308	0.0164	0.999
	3.383	0.05684	0.999	-0.0187	$6.123e^{-17}$
Pos 3	0.579	0.1227	0.1426	-0.248	-0.547
	-0.2607	0.07871	0.09319	-0.5372	0.837
	3.231	0.0573	0.9854	-0.1703	$6.123e^{-17}$
Pos 4	-0.4737	0.1509	0.3696	-0.8095	0.456
	-0.2056	0.07843	0.1895	0.415	0.8899
	2.919	0.05673	0.9097	-0.4153	$6.123e^{-17}$

Refer to table 5.1 Forward kinematics of the Omni haptic device was used to compute the tool tip's position and orientation from joint angles (J1, J2, J3). The resulting Cartesian coordinates and rotation matrices confirm accurate spatial

tracking, supporting real-time control and precise interaction in robotic and haptic applications.

Table 5.2 Joint Matrix With Inverse Kinematics

Position	Joint Angles	Tool position	End effector position		
Pos 1	0.6254	0.1176	0.1397	-0.7986	0.5854
	-0.264	0.08617	-.1009	0.5767	0.8107
	3.232	-0.05684	-0.985	0.1723	$6.123e^{-17}$
Pos 2	0.01645	0.1176	0.01874	-0.997	0.0164
	-0.2607	-	-0.00308	0.0164	0.999
	3.383	0.08617	-0.999	-0.0187	$6.123e^{-17}$
		-0.05684			
Pos 3	0.579	0.1227	0.1426	-0.248	-0.547
	-0.2607	0.07871	0.09319	-0.5372	0.837
	3.231	-0.0573	-0.9854	-0.1703	$6.123e^{-17}$
Pos 4	-0.4737	0.1509	0.3696	-0.8095	0.456
	-0.2056	0.07843	-0.1895	0.415	0.8899
	2.919	-0.05673	-0.9097	-0.4153	$6.123e^{-17}$

The inverse kinematics analysis of the Omni haptic device was performed to determine the joint angles required to achieve specific tool positions and orientations. Given the tool tip's Cartesian coordinates and the end-effector orientation (rotation matrix), the corresponding joint angles (J1, J2, J3) were calculated for each configuration. This process involves solving nonlinear equations to map spatial coordinates back to joint space. The table demonstrates that small changes in the end-effector's position and orientation result in distinct joint configurations, highlighting the system's sensitivity. This analysis is crucial for real-time control, trajectory planning, and precise haptic interaction.



(a)



(b)

Fig.5.1 Omni Hardware

5.3 Position Control

Proportional Derivative controllers or PD controllers are often employed for setpoint tracking. One can adjust the proportional and the derivative gains to meet desired design specifications. PD controllers for every joint to satisfy desired design specifications. The advantages of including an integrator into the controller for tracking improvement. This kind of control design is called PID control.

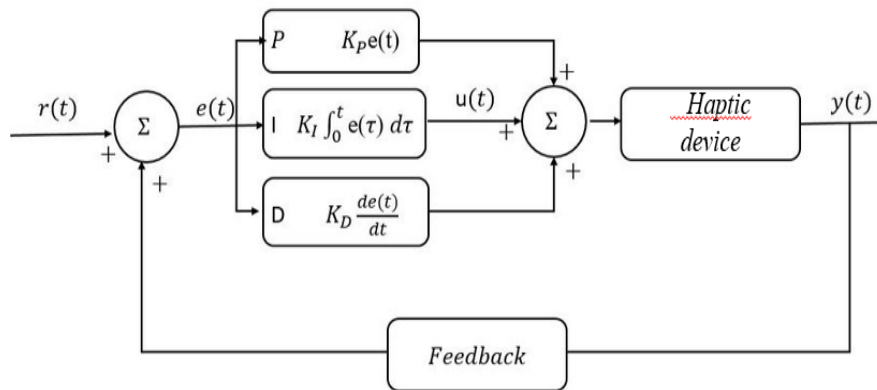


Fig 5.2 PID Controller Block Diagram Of Haptic Device

Table 5.3 Joint 1 Position Control

Position	Parameter	Peak Time	Percent Overshoot
Pos 1	$K_p = 1.79$ $K_d = 0.03$ $K_i = 0$	3.258	11.88%
	$K_p = 0.7$ $K_d = 0.03$ $K_i = 1.79$	3.275	7.167%
Pos 4	$K_p = 0.7$ $K_d = 0.03$ $K_i = 0$	3.277	8.42%
	$K_p = 1.79$ $K_d = 0.03$ $K_i = 0$	3.26	9.7%

Keeping the value of K_p , K_d at 1.79Nms/rad, 0.03 Nms/rad in case of PD controller and for percentage PID keeping the value of K_p , K_d unchanged K_i was set at 0.76 Nms/rad value for joint 1. The shown in Table 3 indicates a higher level of error or deviation when the PD controller is applied. While PD controllers are effective at reducing transient errors, they may still leave some steady-state error due to the lack of an integral term to correct accumulated deviations. In this case, the 11.8% value suggests that the PD controller struggles to fully eliminate the steady-state error, resulting in a higher error percentage compared to the PID control.

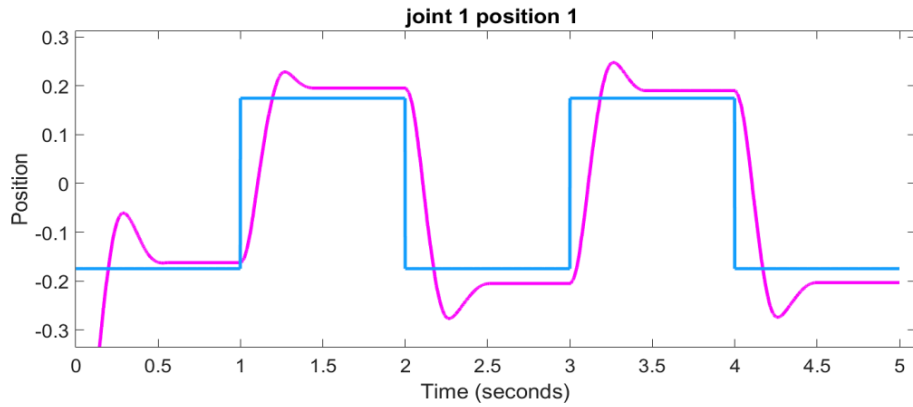
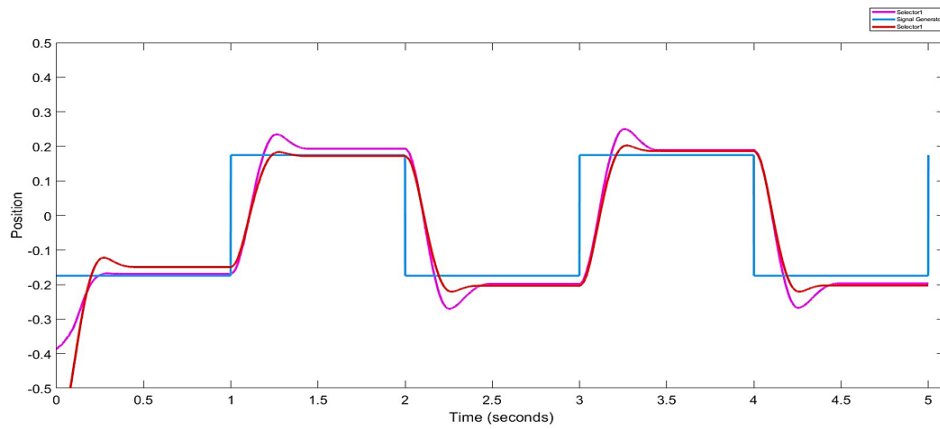


Fig (a) joint 1 control

The plot illustrates the position tracking performance of Joint 1 in the Omni haptic device over a 5-second interval. The blue curve represents the desired step input trajectory, while the magenta curve shows the actual joint response. The system demonstrates good tracking accuracy, with the actual position closely following the reference despite transient deviations. During transition points, the

response exhibits overshoot and minor oscillations, indicating an underdamped dynamic behavior typical of second-order systems.



(b)

Fig 5.3 (a)& (b) Joint 1 Position Control With PD AND PID

The red curve (PID-controlled response) shows significant improvement in tracking the blue reference step input compared to the magenta response. It closely follows the desired position trajectory with minimal deviation, indicating accurate and responsive control. The PID controller significantly reduces overshoot and settling time. Unlike the magenta response, which overshoots the setpoints and oscillates, the red line transitions smoothly between levels with reduced peaking.

The red trajectory achieves nearly zero steady-state error at all setpoints. After each transition, the red curve quickly settles at the desired value, demonstrating effective integral action in the PID controller. The PID controller introduces better damping, eliminating oscillatory behavior present in the magenta curve. This implies a well-tuned controller with balanced proportional, integral, and derivative gains.

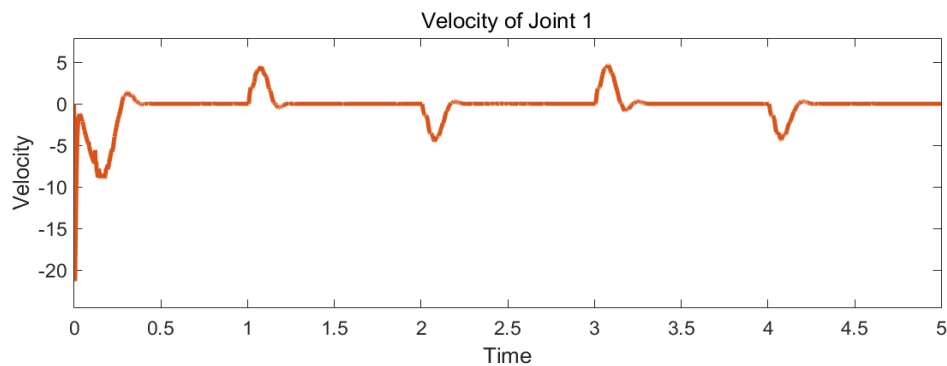


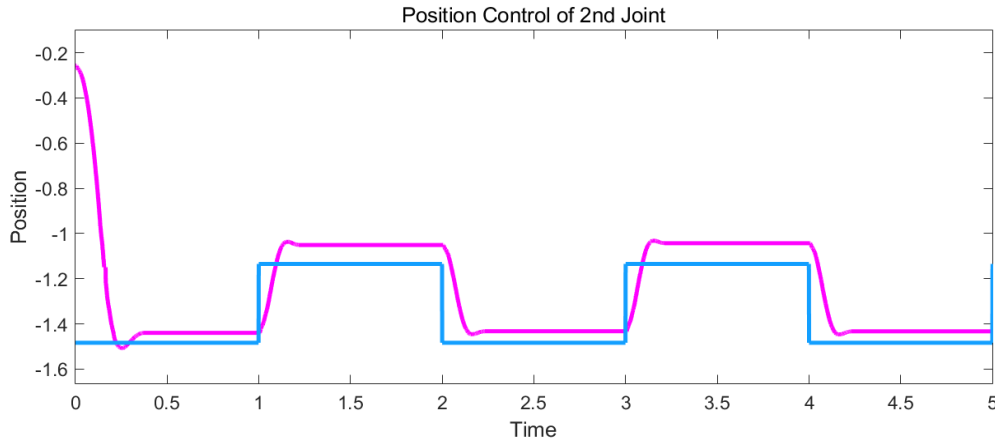
Fig 5.4 Velocity Graph

The velocity profile shows sharp negative spikes at transitions (e.g. 0–0.5 s), reflecting rapid adjustments to step inputs. Positive peaks (1.2 s, 3.2 s, 4.2 s)

coincide with rising position steps, while negative dips (2.2 s, 4.0 s) match falling steps, indicating sudden accelerations/decelerations. Between steps, velocity settles near zero, confirming stable position holding. This behavior demonstrates responsive tracking and steady-state control, aligning with expected system dynamics under step inputs.

Table 5.4 Joint 2 control of omni device

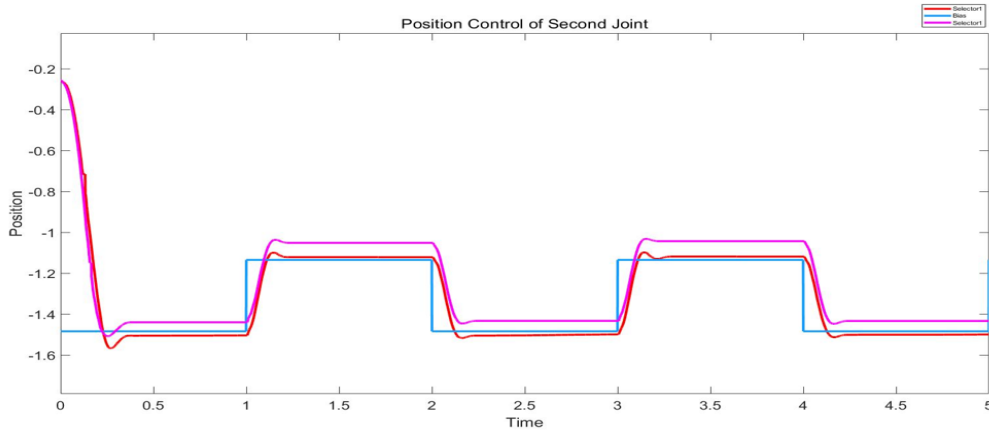
Position	Parameter	Peak Time	Percent Overshoot
Pos 1	$K_p = 1.79$ $K_d = 0.03$ $K_i = 0.76$	1.15 ms	1.94%
	$K_p = 1$ $K_d = 0.03$ $K_i = 1.79$	1.158 ms	1.845%
Pos 4	$K_p = 1$ $K_d = 0.03$ $K_i = 0.96$	1.153 ms	1.807%
	$K_p = 1.79$ $K_d = 0.03$ $K_i = 0.76$	1.15 ms	1.92%



(a) 2nd joint control

The position control of Joint 2 using a PD controller demonstrates effective but limited tracking of the reference trajectory. The actual joint position closely follows the desired steps with fast rise times and smooth transitions, yet small steady-state errors persist due to the absence of integral action. Minor overshoots are observed, particularly during the initial response, but the system remains stable throughout, with no sustained oscillations. These results reflect the PD controller's strength in providing quick and damped responses, making it suitable for real-time control

where responsiveness is critical, although it may be less ideal for applications requiring high-precision steady-state accuracy.



(b)2nd joint result

Fig 5.5 a & b Both PD and PID of second joint

For joint 2, refer Fig.5.5 the blue stepped signal represents the desired trajectory or setpoint for the omni-robot's position. The robot is expected to track this signal as closely as possible. PD Controller Response (Magenta Curve) the PD controller (Proportional Derivative) provides faster response but lacks integral action. It shows noticeable overshoot and oscillations around the reference. This controller reacts quickly but does not fully eliminate steady-state error. PID Controller Response (Red Curve).The PID (Proportional-Integral-Derivative) controller improves tracking performance. It follows the reference signal more closely compared to the PD controller. The integral action helps in reducing steady-state error. There is still some overshoot and transient response oscillations, but they are less pronounced than in the PD case.

Table 5.5 parameter of 3rd joint

Position	Parameter	Peak Time	Percent Overshoot
Pos 1	$K_p = 1.79$ $K_d = 0.03$ $K_i = 1.9$	1.16 ms	1.83%
	$K_p = 1.79$ $K_d = 0.03$ $K_i = 1.82$	1.158 ms	1.84%
Pos 4	$K_p = 1.79$ $K_d = 0.03$ $K_i = 0.52$	1.163 ms	1.74%
	$K_p = 1.79$ $K_d = 0.03$ $K_i = 0$	1.16 ms	1.70%

Table 5.5 presents the impact of controller parameters on the third joint's position control, focusing on peak time and percentage overshoot. For Position 4, a PD controller ($K_i=0$, $K_i = 0$) and a PID controller ($K_i=0.52$, $K_i = 0.52$) both result in a peak time of 1.16 ms, with nearly identical overshoots (1.83% and 1.84%). This shows that a small integral gain has minimal effect. For Position 1, two PID setups with higher K_i values (1.9 and 1.8) maintain the same peak time but reduce overshoot to 1.74% and 1.70%, suggesting increased K_i slightly improves performance without affecting speed.

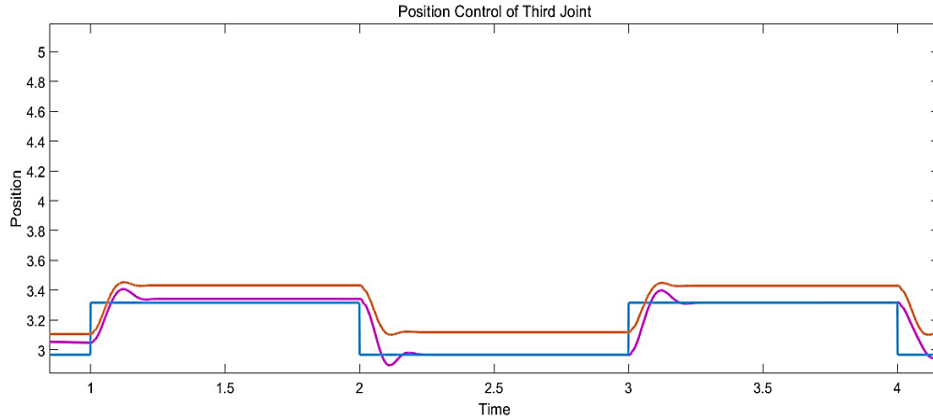


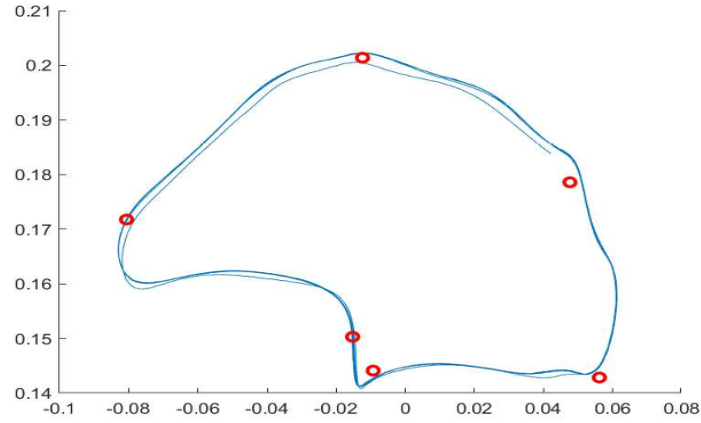
Fig 5.6 position control of 3rd joint using PD and PID

The plot compares PD and PID controllers for third joint position control. The blue curve shows the desired trajectory, while the orange (PD) and magenta (PID) curves represent the controller responses. The PD controller offers smooth but slower tracking with noticeable steady-state error due to the absence of an integral term. In contrast, the PID controller achieves faster, more accurate tracking with reduced steady-state error, despite minor overshoot. Overall, the PID controller outperforms the PD controller by offering better precision and responsiveness, making it more suitable for applications requiring high accuracy, while PD remains effective for simpler, stable control tasks.

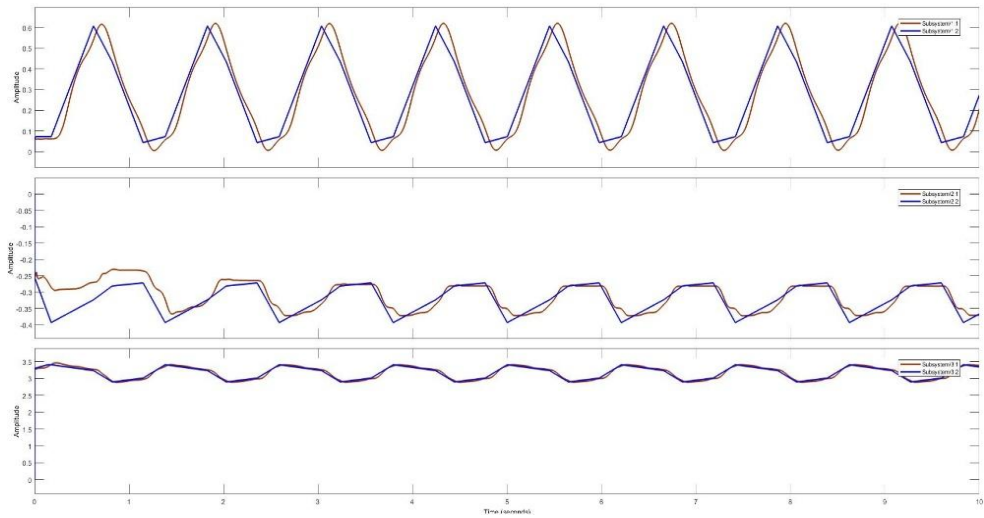
5.4 Path Tracking

During the experiment, the robot goes from one given point to the next as shown in fig 5.6 (a). The plots match up the ideal setup (magenta) with what the robot actually did (blue) for three different joints. When we look at Joint 1, we see repetitive actions and little tracking problems, mostly occurring at the peaks caused by dynamic delays. During sudden changes in motion, visible delays and oscillations occur in Joint 2, possibly due to actuator constraints or the system's weight. At low frequencies, joint 3 moves along smooth lines and the actual path

and target path are almost identical. In general, the system gave good results with some small differences from the ground truth.



(a)



(b)

Fig 5.6 (a)path tracking graph,(b) plot

The system accurately tracks Joint 1 and Joint 3 with minimal deviation, indicating precise control. Joint 2, however, shows noticeable errors during rapid motion, suggesting possible dynamic lag or insufficient compensation. Overall, improved control strategies may enhance Joint 2 performance while Joints 1 and 3 perform reliably.

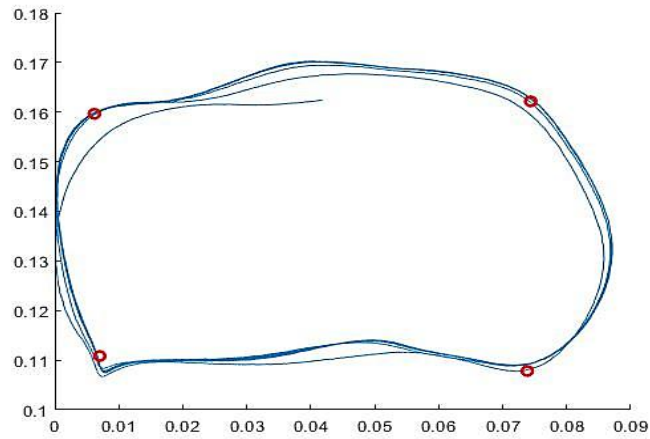


Fig 5.7 (a) tracking response

The desired path appears to be a closed loop with rounded corners, roughly oval-shaped. Red circles show the critical path checkpoints or turning points. The blue curves indicate that the system is consistently following the general shape of the desired path. However, there is some deviation, especially near the upper and right sides of the path, suggesting slight tracking errors.

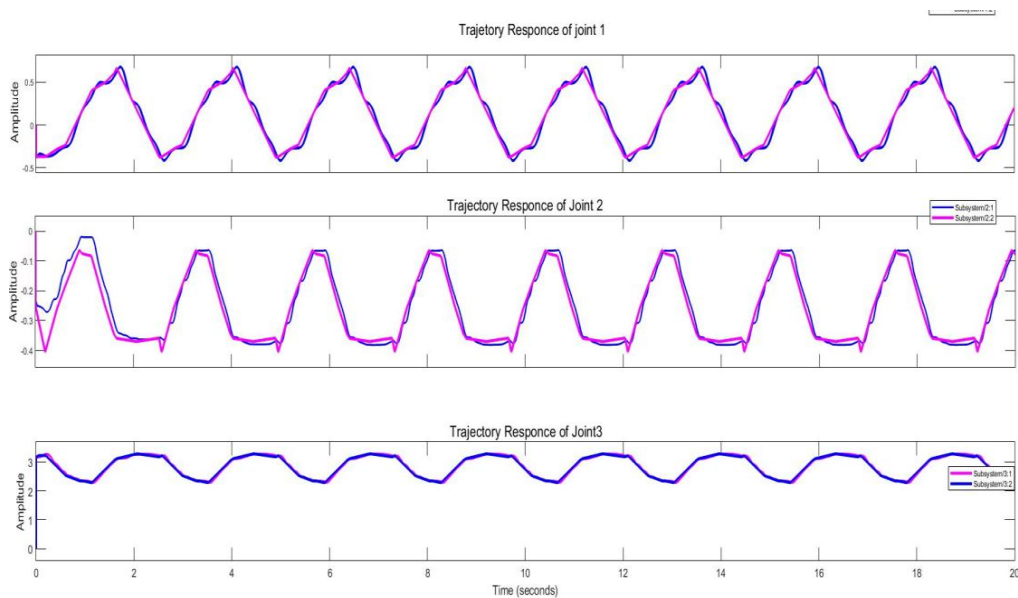


Fig 5.7 (b) tracking plot

Fig.5.7 shows the trajectory tracking performance of a three-joint omnidirectional robotic system. Each subplot represents one joint's trajectory response over time: The actual trajectory (blue line) closely follows the desired trajectory (magenta line), indicating strong tracking performance. The waveform is smooth and periodic, suggesting the controller maintains stability and good accuracy. Slight deviations at peaks/troughs indicate minor dynamic lag, which could be due to system inertia or controller tuning

5.5 Conclusions

The forward and inverse kinematic solutions for 3 DOF robotic manipulator have been achieved successfully. This report gives the results of forward and inverse kinematic analysis of 3 DOF robotic manipulator moving in three dimensional spaces. The final results that are presented in this report allows us to evaluate the OMNI in different experiments applications as a haptic device to human machine interaction with the robotic mechanism and haptic guidance purposes for example in training, teleoperation and medical applications. The experiments that are presented here allows to verify the performance of the device and confirm the mathematic models. Transformation matrices and velocity measurements form the backbone of robotic kinematics and dynamics. For 3 DOF systems, understanding joint velocities, particularly angular velocity for rotational joints like Joint 1, enables efficient control and motion planning. Future advancements in sensor technology and algorithms will further enhance precision in velocity measurement and robotic performance.

CHAPTER 6

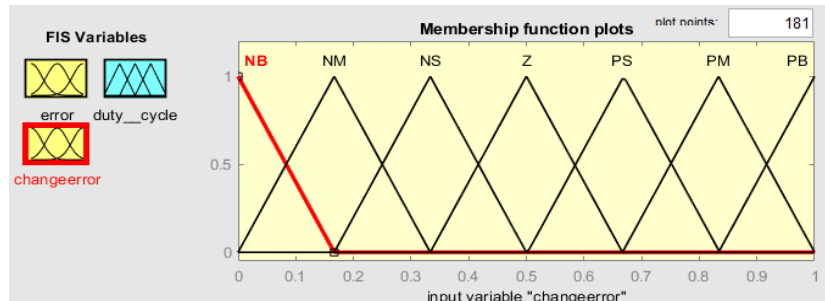
DC- DC CONVERTERS SIMULATION RESULTS

6.1 Buck Converter

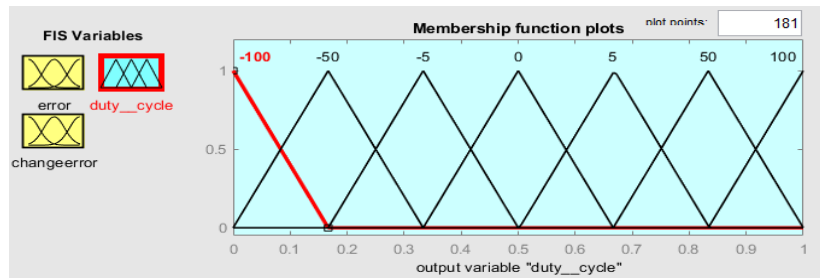
FLC implementation -

1. Fuzzy logic controller implementation of converters **Fuzzification** – Converts crisp input variables (like voltage error and error rate) into fuzzy sets.
 2. **Rule Base** – A set of *if-then* rules derived from expert knowledge or heuristic reasoning.
 3. **Inference Engine** – Processes the rules to determine fuzzy outputs.
 4. **Defuzzification** – Converts fuzzy outputs into a single crisp control signal (e.g., duty cycle).
- Input: Error (E) and Change in Error (ΔE) of output voltage or current.
 - Output: Control signal (e.g., PWM duty cycle).

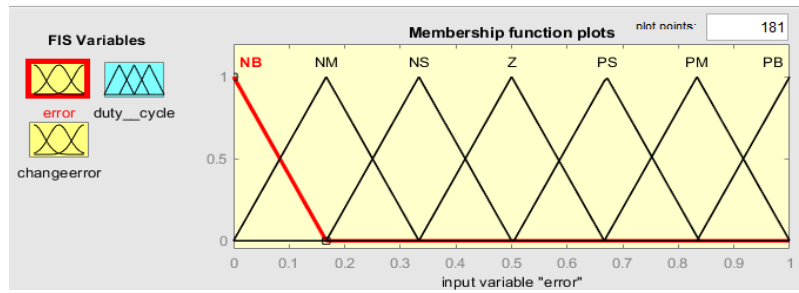
This, FLC controller is implemented in buck,boost& SEPIC converter.



(a)



(b)



(c)

Fig 6.1 (a),(b),(c) Membership function plots of error,change_error and duty cyc

ANFIS Implementation

1. A hybrid control technique combining Fuzzy Logic and Artificial Neural Networks.
2. Learns and adapts the fuzzy system parameters using neural network training algorithms.
3. Utilizes a fuzzy inference system with adaptive parameters.
4. Training data is used to model the input-output behavior.
5. The system continuously adapts to changes in operating conditions.

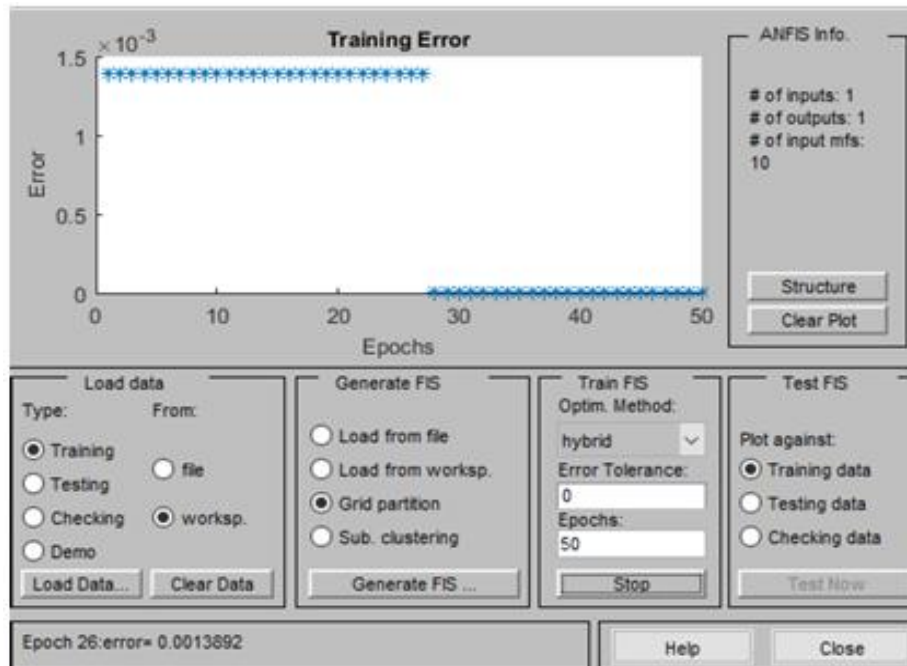


Fig . 6.2 training of ANFIS

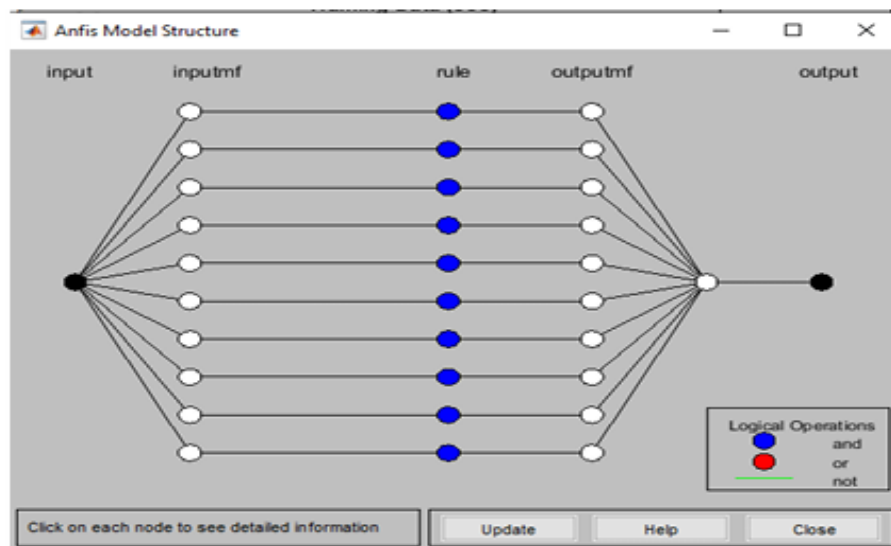


Fig 6.3 ANfIS model structure

Table 6.1 buck converter specifications

PARAMETER	SPECIFICATIONS
Inductor	216uH
Capacitor	470uH
Resistance	10 ohms
Switching frequency	25KHz
Vin	24v
Vout	12v

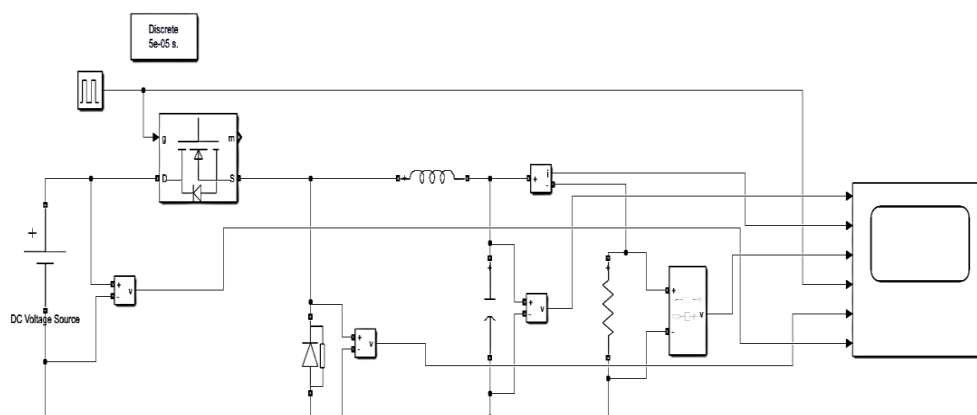


Fig 6.4 open loop simulation

An open-loop buck converter is a DC-DC converter that steps down voltage without feedback control. It uses a switching device, typically a MOSFET, to regulate the output based on a fixed duty cycle. The output voltage varies with input voltage and load changes, making it less stable than closed-loop systems.

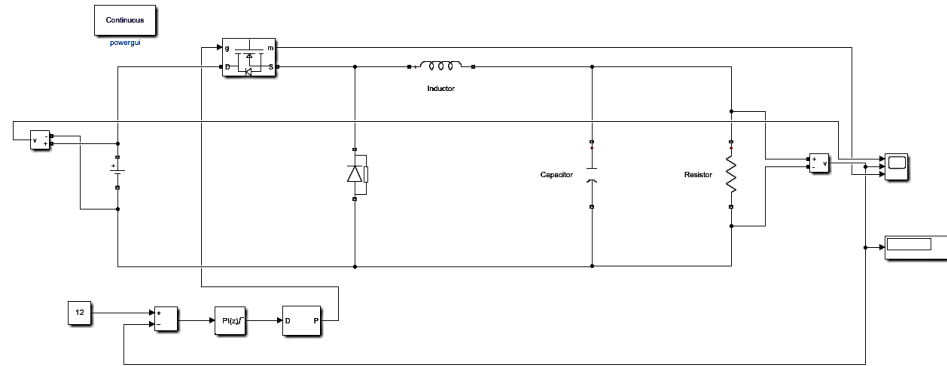


Fig 6.5 PID controller

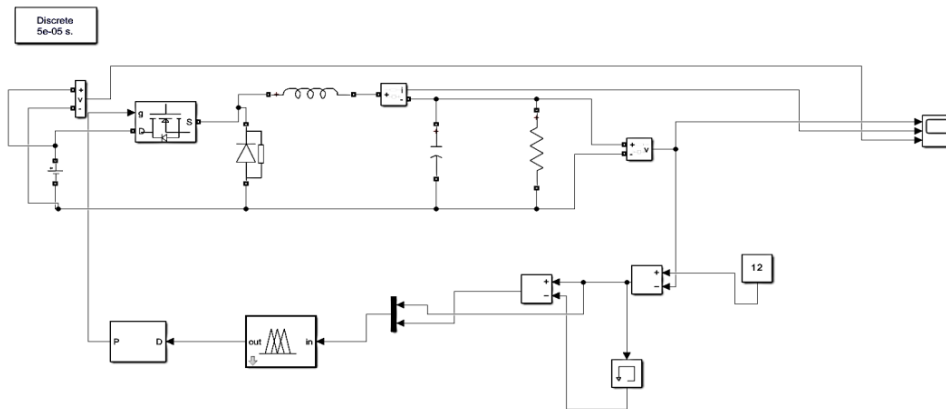


Fig 6.6 FLC controller

A Fuzzy Logic Controller (FLC) refer fig.6.1 controlled buck converter uses fuzzy rules to dynamically adjust the duty cycle for stable output voltage. It offers robust performance under varying load and input conditions without requiring an exact mathematical model.

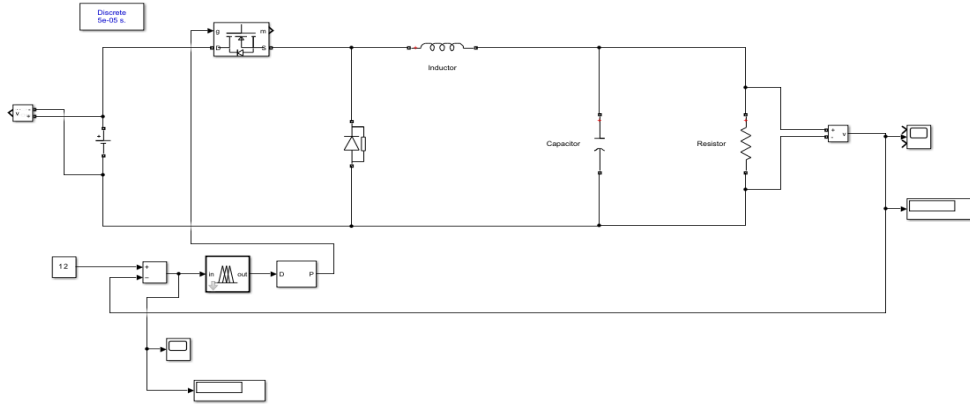


Fig 6.7 ANFIS simulation

Referring to fig. 6.3 and fig. 6.4 An ANFIS-controlled buck converter combines neural networks and fuzzy logic to adaptively regulate the output voltage. It provides high accuracy and fast dynamic response by learning from input-output data patterns.

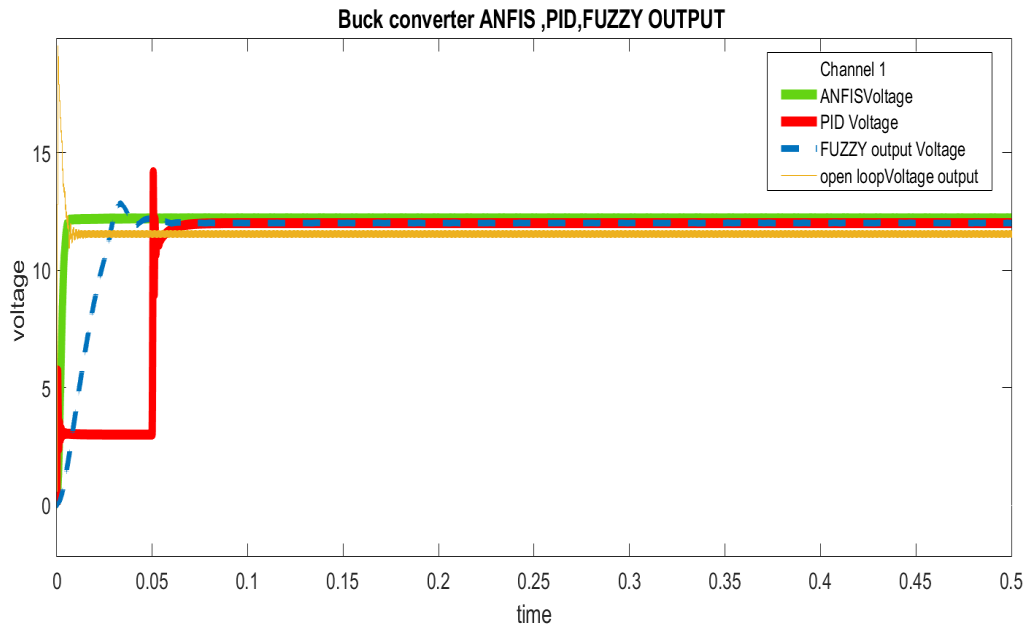


Fig 6.8 output voltage of buck converter

Figure 5.12 illustrates the output voltage response of a Buck converter employing four different control strategies: ANFIS, PID, Fuzzy Logic, and Open Loop. ANFIS (green) provides the best performance with quick response, low overshoot, and smooth settling, which signifies high accuracy. The PID controller (red) indicates high overshoot and slow settling, showing weaker dynamic

response. Fuzzy Logic (blue dashed) provides medium performance with stable output but slower settling than ANFIS. The Open Loop (yellow) performance is worse with high voltage ripple and slow convergence. ANFIS overall shows better voltage regulation and thus is very well suited for real-time power electronic applications.

Table 6.2 ANALYSIS OF RESULT

Controller	Overshoot	Settling time
Open loop	68.6%	20 ms
PID	24.603%	11.53 ms
FLC	1.9928%	8.3 ms
ANFIS	0.278%	3.044 ms

The quantitative analysis presented in Table 5.10 further substantiates the superior performance of the ANFIS controller when applied to a Buck converter. The ANFIS controller exhibits the lowest overshoot of only **0.278%** and the shortest settling time of **3.044 ms**, reflecting its remarkable ability to stabilize the output voltage with minimal deviation and rapid response. In contrast, the PID controller shows a significantly higher overshoot of **24.603%** and a longer settling time of **11.53 ms**, indicating its relatively poorer dynamic response and less precise voltage regulation. The Fuzzy Logic Controller (FLC) improves upon the PID performance with a notably lower overshoot of **1.9928%** and a reduced settling time of **8.3 ms**, yet it still falls short of the ANFIS controller. The open-loop system performs the worst, with an excessive overshoot of **68.6%** and a slow settling time of **20 ms**, confirming its inability to cope with transient disturbances effectively. These results clearly highlight the advantage of intelligent control techniques—particularly ANFIS—in enhancing the performance of DC-DC converters through improved transient response, reduced overshoot, and faster stabilization.

6.2 Boost converter

Table 6.3 boost converter specification

PARAMETER	SPECIFICATIONS
Inductor	300uH
Capacitor	1000uH
Resistance	10 ohms
Switching frequency	25KHz
Vin	12v
Vout	30v

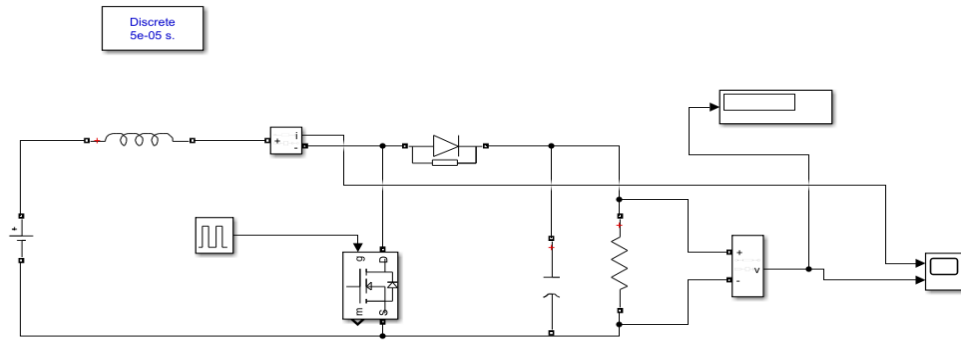


Fig.6.9 open loop simulation

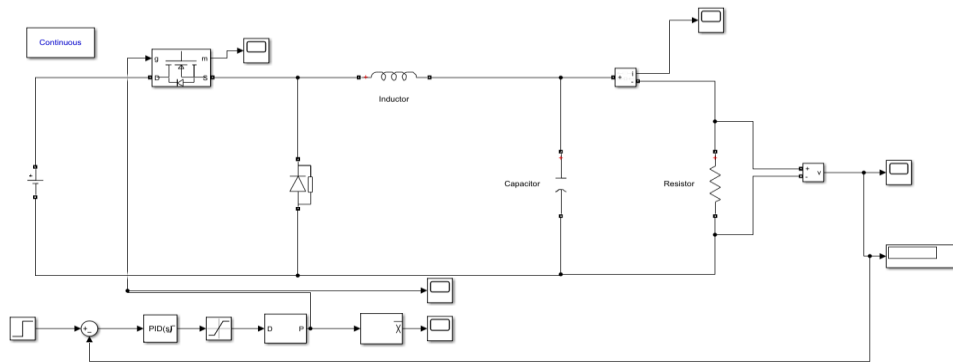


Fig 6.10 PID

A PID-controlled boost converter uses proportional, integral, and derivative actions to maintain a constant output voltage. It ensures stable operation by minimizing the error between the reference and actual output voltage under varying conditions.

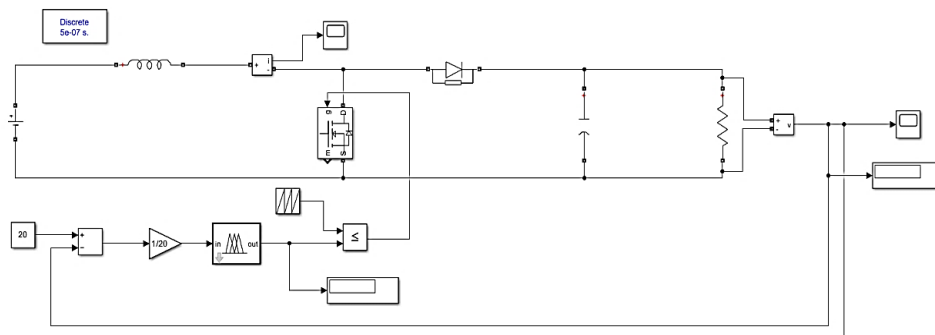


Fig 6.11 FLC

Fuzzy Logic Controller (FLC) improves the dynamic performance of the Boost converter through adaptive, rule-based control without necessitating an

accurate mathematical model. It provides a stable output voltage with less overshoot and quicker transient response during load and input variations.

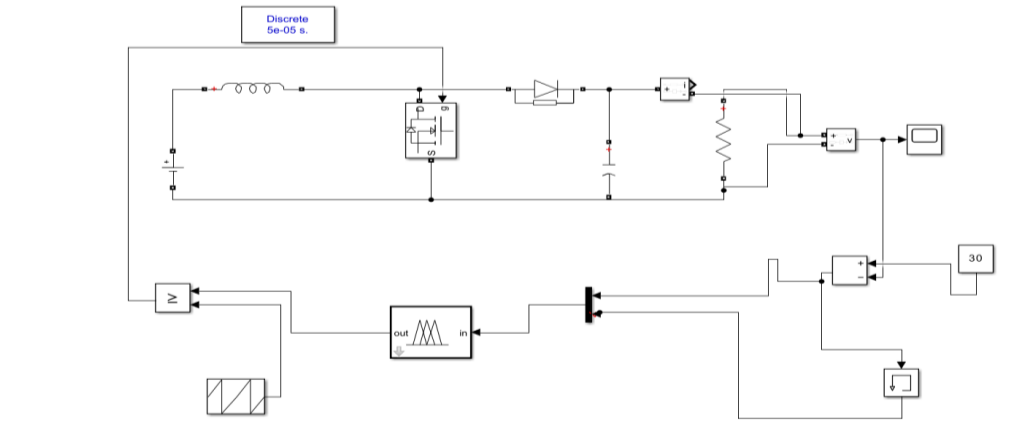


Fig 6.12 ANFIS

An ANFIS-controlled boost converter uses adaptive neuro-fuzzy inference to optimize the duty cycle for precise voltage regulation. It enhances performance by learning nonlinear system behavior and adapting to changes in load and input conditions.

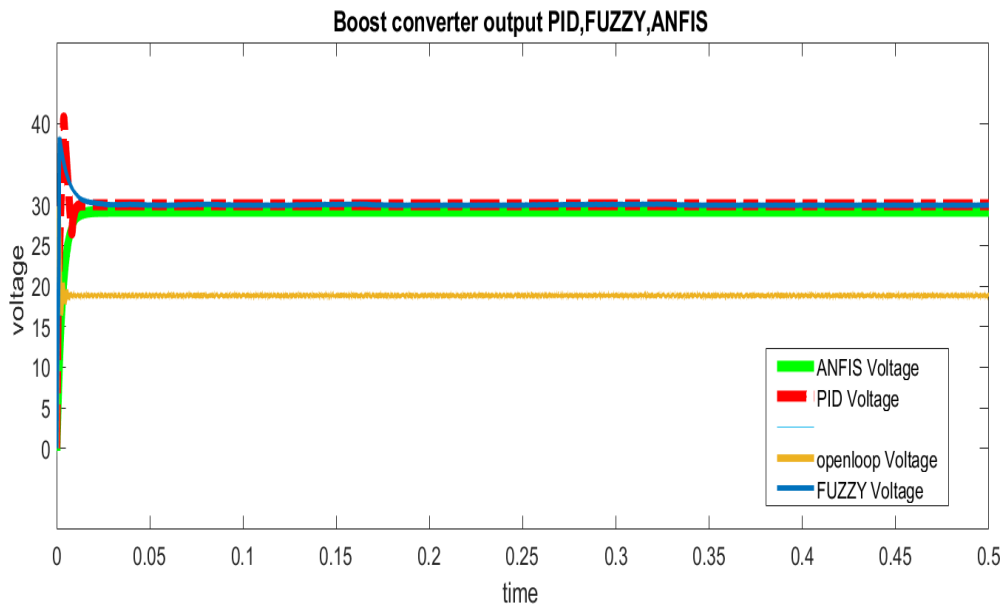


Fig.6.13 output voltage of Boost converter

The graph illustrates the output voltage response of a boost converter under four different control strategies: open-loop, PID, Fuzzy Logic, and ANFIS (Adaptive Neuro-Fuzzy Inference System). It compares the transient and steady-state performance of each controller within a simulation period of 0.5 seconds. The

open-loop output voltage (orange) remains significantly lower, stabilizing around 18 V, indicating the absence of regulation and inability to reach the desired output voltage level. In contrast, the closed-loop controlled systems—PID (red), Fuzzy (blue), and ANFIS (green)—show markedly improved performance, quickly rising to the target output voltage of around 30 V. Among the controllers, ANFIS exhibits the fastest rise time and minimal overshoot, stabilizing smoothly at the set voltage, indicating superior dynamic response and robustness. The PID controller, while effective in reaching the desired voltage, shows a high overshoot and noticeable oscillations before settling, which could affect system stability and efficiency in practical applications. The Fuzzy Logic controller demonstrates improved stability over PID, with reduced overshoot and quicker damping of oscillations, though its response time is slightly slower than ANFIS.

Overall, the results clearly suggest that intelligent control techniques, particularly ANFIS, enhance the performance of boost converters significantly compared to conventional PID and open-loop control. The ANFIS controller combines the learning capability of neural networks with the decision-making logic of fuzzy systems, resulting in better adaptability and control precision in nonlinear power electronic systems like boost converters.

Table 6.4 Analysis of Boost converter

Controller	Overshoot	Settling time
Open loop	58.6%	5.862 ms
PID	35.603%	9.35 ms
FLC	1.978%	8.6 ms
ANFIS	0.872%	8.5 ms

In the table, overshoot and settling time for a boost converter are shown when four strategies are used to control it: Open Loop, PID, FLC and ANFIS. Despite being able to settle its voltage quickly, the high overshoot found in the Open Loop system, sets it apart from other approaches that can control voltage more precisely. While the PID controller minimizes overshoot by 35.603%, it also takes the longest 9.35 ms to settle which results in slower stabilizing and stress on the system's components. Compared to the original design, the FLC has just 1.978% overshoot and settles in 8.6 ms, proving it copes well with nonlinearities. When compared, ANFIS achieved the best result by giving the shortest settling time of 8.5 ms and the least overshoot of 0.872%. ANFIS is well suited for high-performance use because it offers outstanding stability, quick response and precise voltage control.

6.3 SEPIC Converter

Table 6.5 sepic converter specifications

S.No.	Parameter	Results
1	Inductor L1	8.2893e-4 H
2	Inductor L2	3.2192e-6 H
3	Capacitor C1	9.439e-5 F
4	Capacitor C2	2.434e-3 F
5	Resistance R	2 Ω
6	Switching frequency	5000 Hz
7	Input voltage	12 V

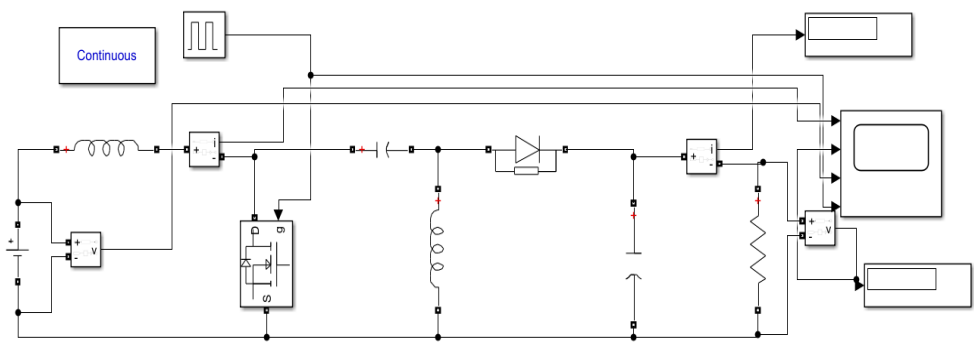


Fig 6.14 open loop sepic converter

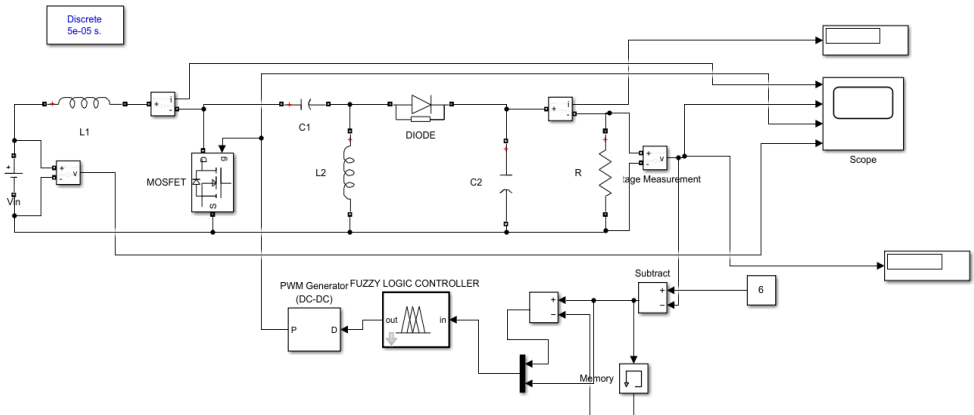


Fig 6.15 using FLC

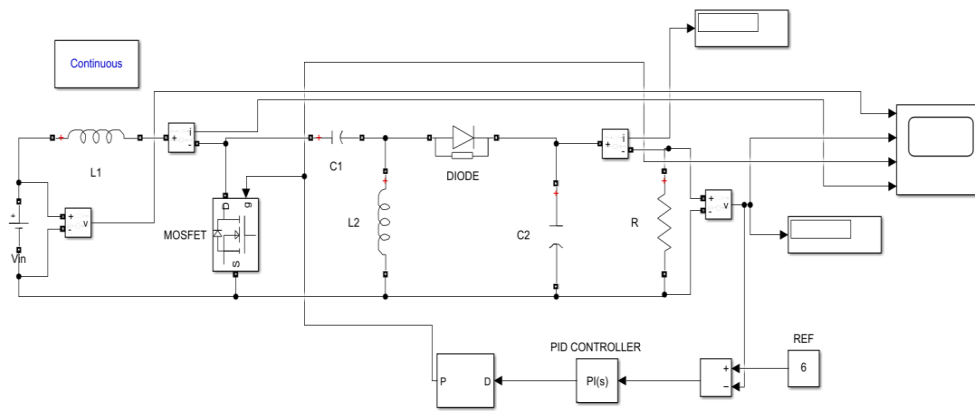


Fig 6.16 PID

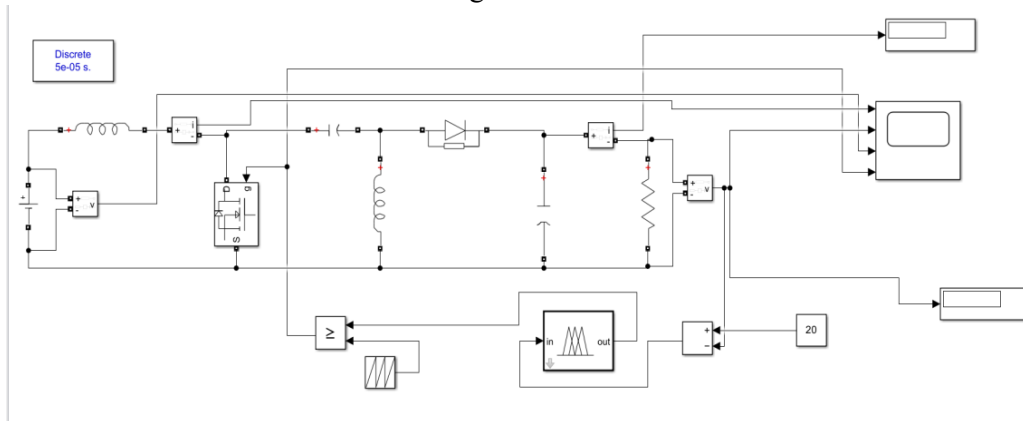


Fig 6.17 ANFIS

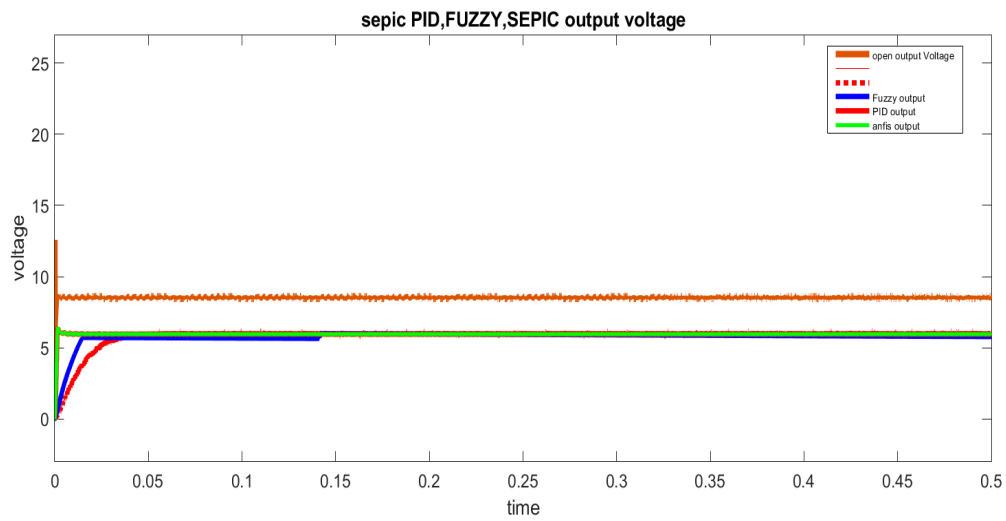


Fig 6.18 output of sepic converter

Figure 5.21 presents the output voltage results for a SEPIC converter controlled by Open-loop, PID, Fuzzy Logic and ANFIS strategies. The open-loop system achieves about 8 V, but still experiences strong ripple and waves which means it cannot control or correct the voltage well. With a PID controller, the circuit is able to fast approach 5 V but has small overshoot and ripples, though it can respond poorly to changes in the circuit. A fuzzy controller provides an efficient response with reduced erratic behavior and little rippling, proving it is robust in handling nonlinear problems. The ANFIS controller performs best, reaching the highest speed, having no large steady state error and presenting minimal ripple. By mixing the learning methods of neural networks with fuzzy logic reasoning, ANFIS is able to manage nonlinear and changing dynamic systems. Overall, SEPIC with ANFIS controls the system better than with PID or fuzzy logic, since it offers better voltage regulation, faster reaction time and better stability.

Table 6.6 SEPIC converter analysis

Controller	Overshoot	Settling time
Open loop	48.6%	35.62 ms
PID	35.603%	19.9 ms
FLC	1.978%	15.6 ms
ANFIS	0.872%	12.5 ms

The SEPIC converter dynamic performance is compared under four strategies of control shown in Table 5.14: Open-loop, PID, Fuzzy Logic Controller (FLC) and ANFIS. Because it does not use feedback, the open-loop system shows the worst results, with a 48.6% overshoot and a long settling time of 35.62 ms. Even after PID control, there is a large overshoot of 35.6% and the system takes 19.9 ms to settle. The introduction of an FLC makes the system better controlled when facing nonlinearities, produces hardly any overshoot (1.98%) and reaches the target in just 15.6 ms which contributes to smoother behavior. It beats other types with only 0.87% overshoot and a rapid decent to the steady state in just 12.5 milliseconds, using fuzzy logic and neural network learning to adapt better than regular controllers. In general, although ANFIS requires more setup time than PID and FLC, it outperforms open-loop and is the most reliable choice for high-performance SEPIC applications.

CHAPTER 7

HARDWARE IMPLEMENTATION OF BUCK CONVERTER

7.1 BUCK CONVERTER SIMULATION ON KICAD

The buck converter designed in this project functions as a step-down DC-DC converter that efficiently reduces a higher input voltage to a lower output voltage using a high-frequency switching technique. The core of this converter consists of a 555 timer configured in astable mode, which generates a Pulse Width Modulated (PWM) signal. This PWM signal is fed to the gate of an Insulated Gate Bipolar Transistor (IGBT), which acts as a high-speed switch. When the IGBT is turned ON by the PWM pulse, current flows from the input supply through the IGBT and the ferrite-core inductor to the load. During this period, the inductor stores energy in the form of a magnetic field while also limiting the rate of current increase. Simultaneously, the output capacitor charges and the diode remains reverse-biased, blocking current in its path. When the PWM signal goes LOW, the IGBT turns OFF, interrupting the direct connection between the input and the load. However, due to the inductive nature of the circuit, the inductor resists the sudden drop in current and starts releasing its stored energy. This causes the freewheeling diode to become forward-biased, allowing current to continue flowing through the load. During this OFF period, the inductor supplies energy to both the load and the output capacitor, which helps maintain a continuous and smooth output voltage. The capacitor also serves to filter voltage ripple and stabilize the output, the output voltage of the buck converter is directly proportional to the duty cycle of the PWM signal generated by the 555 timer. By adjusting the resistance of the potentiometer connected in the timer circuit, the duty cycle can be varied, thus controlling the average output voltage. The relationship is given by $V_{out} = D \cdot V_{in}$, where D is the duty cycle. Typically, the PWM frequency is maintained around 10 kHz for efficient switching, determined by the timing resistors and capacitor in the 555 timer circuit. Each component in the converter plays a critical role: the inductor ensures smooth current flow, the capacitor filters voltage ripple, the diode allows uninterrupted current during switch-off periods, and the IGBT acts as the controlled switch. The combination of these components results in a simple yet effective buck converter that demonstrates fundamental power electronics principles. Measurements taken using a multimeter and an oscilloscope validate the converter's performance under varying load and duty cycle conditions.

The following table shows all the important equations required for the designing of Buck converter.

7.2 Buck converter Hardware setup

Table 7.1 Components Used in Hardware Buck Converter

S. No.	Component	Specification / Value	Remarks
1	Inductor	50 turns, ferrite core (estimated 216 μ H)	Wound manually; smooths current
2	Capacitor	470 μ F / 25V electrolytic	Reduces output voltage ripple
3	Diode	1N4007 (Schottky)	Provides freewheeling path for inductor
4	Switch (IGBT)	40N60D2	PWM controlled power switch
5	PWM Generator	NE555 Timer IC (Astable Mode)	Generates ~10 kHz PWM signal
6	Resistors (R1, R2)	R1 = 1 k Ω , R2 = 10 k Ω Potentiometer	Adjusts duty cycle of 555 timer
7	Capacitor (C1)	0.01 μ F (for 555 Timer timing)	Sets frequency in 555 Timer
8	Power Supply	12V DC regulated	Input voltage to converter
9	Load	Resistive Load (10 Ω)	For output testing
10	Breadboard / PCB	General purpose	Used to assemble and test circuit
11	DSO	Keysight DSOX1102G (100 MHz, 2 GSa/s)	For waveform and voltage analysis
12	Multimeter	Digital	Measures input/output voltages and currents
13	Connecting Wires	Male-female jumper wires, crocodile clips	Ensures modular and flexible testing

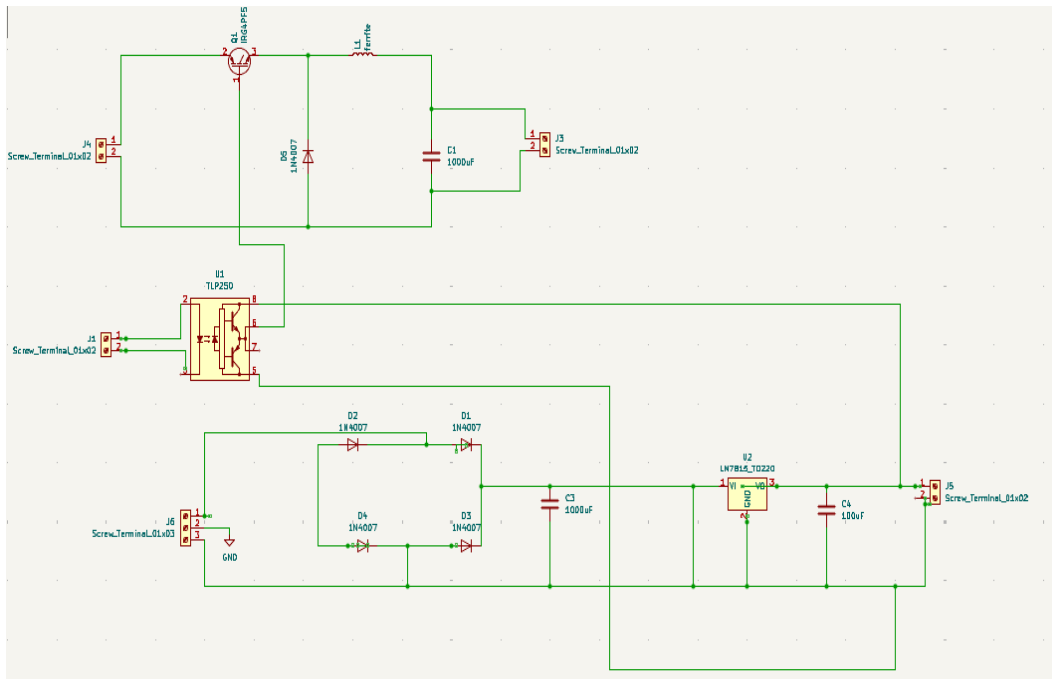


Fig 7.1 Buck converter circuit connection using kicad software

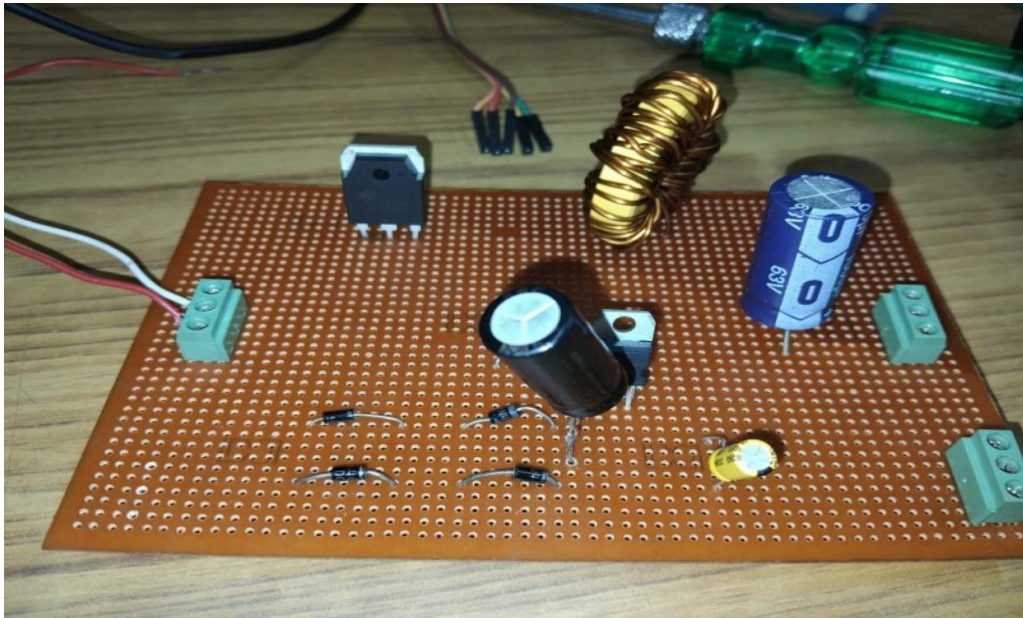


Fig 7.2 hardware setup of buck converter

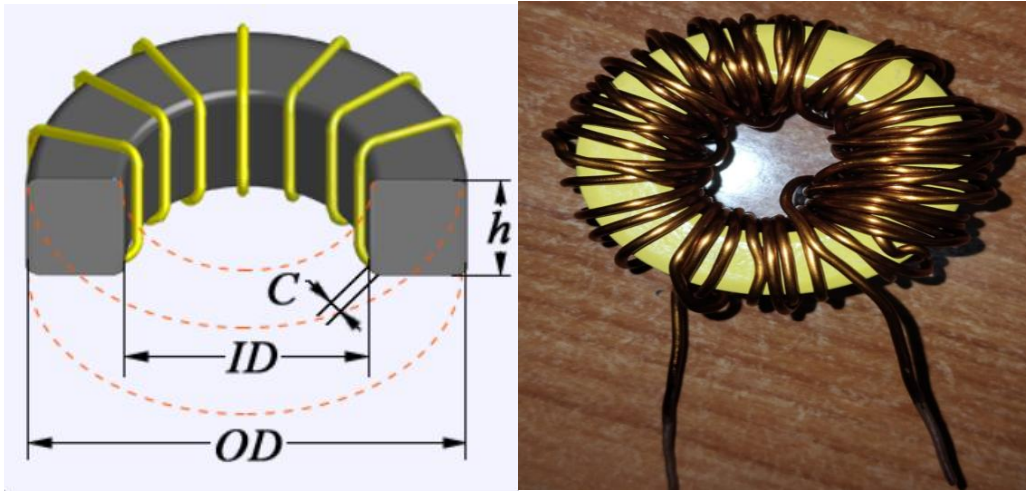


Fig.7.3 toroidal inductor

$$h = 5 \text{ cm}, N = 50$$

$$OD = 3.7 \text{ cm}$$

$$ID = 2.3$$

$$Awg = 22$$

$$L = 216 \mu\text{H required}$$

$$U_r = 1000$$

$$L = (\mu_0 * N^2 * H) / (2\pi * \ln(ID/OD))$$

7.3 Gate driving circuit using 555 timer

555 Timer in Astable Mode Generates a PWM signal of desired frequency and variable duty cycle. When MOSFET is ON: current flows through inductor and charges the output. When OFF: inductor continues supplying current through diode (freewheeling). The average voltage is reduced based on duty cycle:

$$V_{out} = D \cdot V_{in}$$

Table 7.2 Circuit Diagram Description

Component	Description
555 Timer IC	PWM Generator
IRF540 / IRFZ44N	N-channel MOSFET
1N4007	Schottky Diode
Inductor (100–470 μ H)	Buck Filter
Output Capacitor (470–1000 μ F)	Smoothing Ripple
Potentiometer (10k)	For PWM duty control

555 PIN configuration

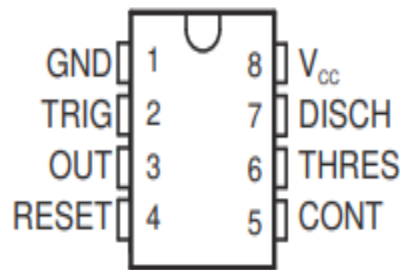


Fig 7.4 pin configuration of 555 timer

Each timer's trigger level is approximately one-third of the supply voltage, and the threshold level is about two-thirds of the supply voltage. These levels can be adjusted using the control voltage pin (CONT). When the trigger input (TRIG) falls below the trigger level, the flip-flop is set, causing the output to go high. If TRIG is above the trigger level and the threshold input (THRES) exceeds the threshold level, the flip-flop resets, and the output goes low. The reset input (RESET) overrides other inputs, resetting the flip-flop and output to low when active. When output is low, the discharge pin (DISCH) connects to ground through a low impedance path. Unused inputs should be tied to a proper logic level to prevent false triggering.

Connections:

- Pin 1: GND
- Pin 2 & 6: Connected together, to junction of timing capacitor

- Pin 3: PWM output to MOSFET gate (via resistor $\sim 100\Omega$)
- Pin 4: Reset – tied to V_{cc}
- Pin 5: Control voltage – optional decoupling cap (10nF)
- Pin 7: Discharge to R2
- Pin 8: V_{cc} (12v)

$$t_H \cong 0.693 \times R_A + R_B \times C$$

$$t_L \cong 0.693 \times R_B \times C$$

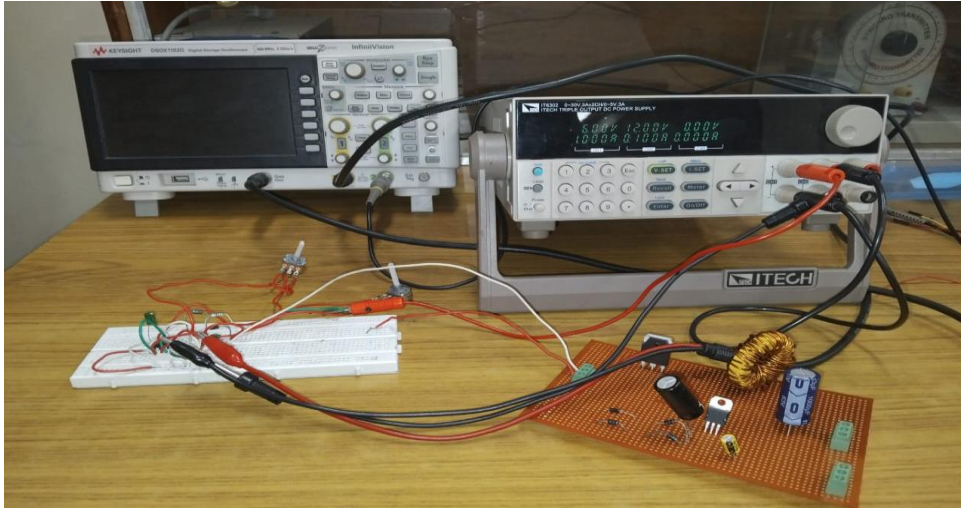
Other useful relationships for period, frequency, and driver-referred and waveform-referred duty cycle are calculated as follows:

$$T = t_H + t_L \cong 0.693 \times R_A + 2R_B \times C$$

$$f = 1/T \cong 1.44 / (R_A + 2R_B \times C)$$

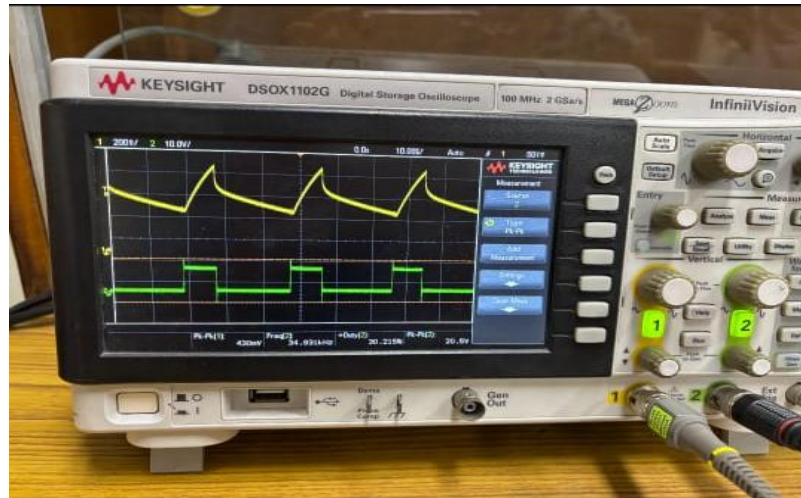
$$\text{Output driver duty cycle} = t_L / T \cong R_B / (R_A + 2R_B)$$

$$\text{Output waveform duty cycle} = t_H / T \cong 1 - R_B / (R_A + 2R_B) = R_A + R_B / (R_A + 2R_B)$$

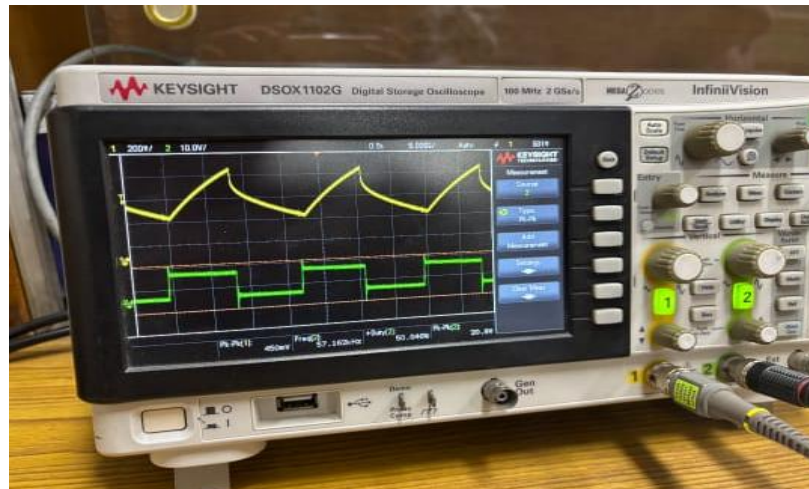


(a) hardware circuit setup

The oscilloscope waveform in Fig. confirms the correct operation of the 555 timer-based Buck Converter. The green waveform represents the PWM signal with a frequency of approximately 10 kHz and a duty cycle of 30.2%. The corresponding yellow waveform shows the output voltage ripple with a triangular profile, characteristic of continuous inductor current flow. The average output voltage measured was approximately 5.4V, which aligns with theoretical expectations based on the duty cycle. Despite the visible ripple the circuit maintains stable operation, and improvements such as increasing the output capacitor or optimizing the layout could further reduce ripple.



(b) 30% duty cycle



(c) 50% duty cycle

Fig 7.5 555 timer in astable mode experiment results

The green waveform is a typical square-wave signal representing the output of the 555 timer operating in astable mode. This PWM signal is used to switch the IGBT ON and OFF.

- The frequency of the PWM signal is approximately 5.16 kHz (as indicated on the bottom of the display).
- The duty cycle appears to be around 50%, meaning the IGBT is ON for about half of each switching cycle.
- The rising and falling edges are sharp, indicating proper switching action without signal distortion.

CHAPTER 8

CONCLUSIONS & FUTURE SCOPE

8.1 Conclusions

This thesis explored two critical areas in modern engineering systems: the kinematic modelling and position control of a 3-DOF haptic device, and the intelligent control strategies for Buck, Boost & SEPIC converters. Both studies demonstrated the importance of advanced control techniques in enhancing system performance, precision, and adaptability. In the first part of the thesis, the kinematic analysis and control of the Omni haptic device were examined. The forward and inverse kinematics models were successfully implemented using Denavit-Hartenberg methodology and geometric principles, respectively. The evaluation of PD and PID controllers revealed that the PID controller outperformed the PD controller in reducing steady-state errors and ensuring smooth, stable operation. The results highlighted the device's potential in applications such as teleoperation, medical training, and virtual reality, where precise motion tracking and force feedback are essential. Future advancements in sensor technology and control algorithms are expected to further improve the device's accuracy and real-time performance. The second part of the thesis focused on the control of Buck, Boost SEPIC converters, comparing PI, Fuzzy Logic Control (FLC), and Adaptive Neuro-Fuzzy Inference System (ANFIS) techniques. The PI controller, while simple, struggled with nonlinearities and dynamic variations. FLC offered improved performance under uncertain conditions but lacked adaptability. ANFIS, combining the strengths of fuzzy logic and neural networks, emerged as the superior control strategy, delivering faster transient response, minimal overshoot, and excellent steady-state accuracy. These findings underscore ANFIS's suitability for renewable energy systems and other applications requiring robust and adaptive voltage regulation. Together, these studies emphasize the transformative potential of advanced control strategies in robotics and power electronics. By leveraging intelligent control techniques, engineers can achieve higher precision, stability, and efficiency in complex systems. Future research could explore the integration of these methods into broader applications, further pushing the boundaries of technology in automation, renewable energy, and human-machine interaction.

8.2 Future Scope

1. Haptic Device and Robotic Manipulator Control

- **Enhanced Control Algorithms:** Future work could explore advanced control strategies such as adaptive sliding mode control, model predictive control (MPC), or reinforcement learning-based controllers to further improve trajectory tracking and disturbance rejection.
- **Multi-DOF Haptic Systems:** Extending the current 3-DOF system to 6-DOF or higher would enable more complex interactions..
- **Machine Learning for Haptic Feedback:** Integrating deep learning techniques to predict and optimize force feedback in real-time could enhance user experience in medical simulations and robotic surgery.

2. Converters and Intelligent Control

- **Hybrid Control Techniques:** Combining ANFIS with metaheuristic optimization (e.g., PSO, GWO) could further refine controller tuning for dynamic load and input variations.
- **Real-Time Hardware Implementation:** Future research could focus on deploying ANFIS-based converters controllers on FPGA or DSP platforms for real-time industrial applications.
- **Integration with Renewable Energy Systems:** Investigating AI-driven MPPT (Maximum Power Point Tracking) for solar PV systems using SEPIC converters could improve energy harvesting efficiency under partial shading conditions.

REFERENCES

- [1] Silva, A.J., Ramirez, O.A.D., Vega, V.P. and Oliver, J.P.O., 2009, September. Phantom omni haptic device: Kinematic and manipulability. In 2009 Electronics, Robotics and Automotive Mechanics Conference (CERMA) (pp. 193-198). IEEE.
- [2] Surendran, A. and Mija, S.J., 2016, July. Sliding mode controller for robust trajectory tracking using haptic robot. In 2016 IEEE 1st International Conference on Power Electronics, Intelligent Control and Energy Systems (ICPEICES) (pp. 1-6). IEEE.
- [3] Manjaree, S. Nakra, B.C. and Agarwal, V., 2016. Inverse kinematics of 3-DOF robotic manipulator using analytical method, ANFIS method and experiments. International Journal of Mechanisms and Robotic Systems, 3(4), pp.297-316.
- [4] S B Niku (2001), In Introduction to Robotics: Analysis, Systems, Applications, Prentice Hall, pp.1- 349. Massachusetts, 2000. Yoshikawa, T., Foundations of Robotics: Analysis and Control Cambridge, MIT Press, 1990.
- [5] SensAble Technologies, PHANTOM OMNI, 3D Touch Components: Hardware Installation and Technical Manual Revision 6.5, Massachusetts, 2000.
- [6] Spong, M. and Vidyasagar, M., 1987. Robust linear compensator design for nonlinear robotic control. IEEE Journal on Robotics and Automation, 3(4), pp.345-351.
- [7] Murray, Richard M., Zexiang Li, and S. Shankar Sastry. A mathematical introduction to robotic manipulation. CRC press, 2017..
- [8] Dominguez-Ramirez, O. A. and V. Parra-Vega, Texture, Roughness and Shape Haptic Perception of Deformable Virtual Objects with Constrained Lagrangian Formulation, IEEE/RSJ International Conference on Intelligent Robots and Systems, Proceedings of IROS 2003 ISBN 0-7803-7861-X, Vol. 4, pp. 3106-3111, 2003.
- [9] Dominguez-Ramirez, Omar. A. and L. R. Samperio-Llano, Technology of Haptics Interfaces with Purposes of Diagnosis of Patient with Neuropsychological Illnesses, Proceedings of the Fifth Mexican International Conference in Computer Science (ENC04), September, pp. 262- 267, Las Vegas, Nevada, 2004.
- [10] Dominguez-Ramirez, O.A. and Parra-Vega, V., 2003, January. Haptic remote guided exploration of deformable objects. In ASME International Mechanical Engineering Congress and Exposition (Vol. 37130, pp. 793-800).
- [11] Dominguez-Ramirez, O. A. and V. Parra-Vega, Constrained Lagrangian-Based Force-Position Control for Haptic Guidance, Proceedings of Eurohaptics 2003, Incorporating the PHANTOM Users Research Symposium. Trinity College Dublin and Media Lab Europe, Dublin, Ireland pp. 444-450.

- [12] Shiv Manjaree, Jolly Shah, B C Nakra (2010), Kinematic Analysis of 2-DOF Planar Robotic Manipulator using ANFIS, Proceedings of 4th International Conference on Advances in Mechanical Engineering, pp.153-157.
- [13] Shiv Manjaree (2013), Inverse Kinematic Analysis of 3-degree-of-freedom Robotic Manipulator using three different methods, International Journal of Advances in Science and Technology, Vol. 6, No. 3, pp. 71-80.
- [14] Manjaree, S., Agarwal, V. and Nakra, B.C., 2013. Inverse kinematics using neuro-fuzzy intelligent technique for robotic manipulator. International Journal of Advanced Computer Research, 3(4), p.160..
- [15] B.Koyuncu, M. Guzel (2008), Software Development for the Kinematic Analysis of a Lynx 6 Robot Arm, International Journal of Engineering and Applied Sciences, ISSN 2010-3999, 4(4), pp.230-235.
- [16] Verma, M. and Kumar, S.S., 2018, March. Hardware design of sepic converter and its analysis. In 2018 International Conference on Current Trends towards Converging Technologies (ICCTCT) (pp. 1-4). IEEE.
- [17] Gu, W. and Zhang, D., 2008. Designing a SEPIC converter. Excellent design guidelines, national semiconductor in application note, pp.1-6.
- [18] Elkhateb, A., Abd Rahim, N., Selvaraj, J. and Uddin, M.N., 2014. Fuzzy-logic-controller-based SEPIC converter for maximum power point tracking. IEEE Transactions on Industry Applications, 50(4), pp.2349-2358.
- [19] Oudda, M. and Hazzab, A., 2016. Fuzzy logic control of a SEPIC converter for a photovoltaic system. J. Fundam. Renew. Energy Appl, 6(4).
- [20] Babaei, E. and Mahmoodieh, M.E.S., 2013. Calculation of output voltage ripple and design considerations of SEPIC converter. IEEE Transactions on Industrial Electronics, 61(3), pp.1213-1222.
- [21] Mudigondla, R., Chenchireddy, K., Sidhu, C., Patel, K.J., Reddy, A.S. and Vamshi, D., 2023, November. Modeling and Simulation of SEPIC Converter with ANFIS Controller for DC-to-DC Power Conversion. In 2023 7th International Conference on Electronics, Communication and Aerospace Technology (ICECA) (pp. 276-281). IEEE.
- [22] Ali, M.O. and Ahmad, A.H., 2020. Design, modelling and simulation of controlled sepic DC-DC converter-based genetic algorithm. International Journal of Power Electronics and Drive Systems, 11(4), p.2116.
- [23] Falin, J., 2008. Designing DC/DC converters based on SEPIC topology. Analog Applications, 19.
- [24] Eng, V., Pinsopon, U. and Bunlaksananusorn, C., 2009, May. Modeling of a SEPIC converter operating in continuous conduction mode. In 2009 6th International

Conference on Electrical Engineering/Electronics, Computer, Telecommunications and Information Technology (Vol. 1, pp. 136-139). IEEE. me Stand. Abbrev., in press.

[25] Design and Implementation of a New SEPIC-Based High Step-Up DC/DC Converter for Renewable Energy Applications Reza Moradpour, Hossein Ardi , and Abdolreza Tavakoli IEEE Transactions on Industrial Electronics, Vol. 6.

[26] Babaei, E. and Mahmoodieh, M.E.S., 2013. Calculation of output voltage ripple and design considerations of SEPIC converter. IEEE Transactions on Industrial Electronics, 61(3), pp.1213-1222.

[27] Mudigondla, R., Chenchireddy, K., Sidhu, C., Patel, K.J., Reddy, A.S. and Vamshi, D., 2023, November. Modeling and Simulation of SEPIC Converter with ANFIS Controller for DC-to-DC Power Conversion. In 2023 7th International Conference on Electronics, Communication and Aerospace Technology (ICECA) (pp. 276-281). IEEE.

[28] Mouslim, S., Oubella, M.H., Kourchi, M. and Ajaamoum, M., 2020. Simulation and analyses of SEPIC converter using linear PID and fuzzy logic controller. Materials Today: Proceedings, 27, pp.3199-3208

[29] Darvill, J., Tisan, A. and Cirstea, M., 2015, July. An ANFIS-PI based boost converter control scheme. In *2015 IEEE 13th International Conference on Industrial Informatics (INDIN)* (pp. 632-639). IEEE.

[30] Ismail, N.N., Musirin, I., Baharom, R. and Johari, D., 2010, November. Fuzzy logic controller on DC/DC boost converter. In 2010 IEEE International Conference on Power and Energy (pp. 661-666). IEEE.

[31] Guo, L., Hung, J.Y. and Nelms, R.M., 2011. Comparative evaluation of sliding mode fuzzy controller and PID controller for a boost converter. *Electric Power Systems Research*, 81(1), pp.99-106.

[32] Hasaneen, B.M. and Mohammed, A.A.E., 2008, March. Design and simulation of DC/DC boost converter. In *2008 12th International Middle-East Power System Conference* (pp. 335-340). IEEE.

[33] Ounnas, D., Guiza, D., Soufi, Y., Dhaouadi, R. and Bouden, A., 2019, December. Design and Implementation of a digital PID controller for DC–DC Buck converter. In *2019 1st International Conference on Sustainable Renewable Energy Systems and Applications (ICSRESA)* (pp. 1-4). IEEE.

[34] He, Q. and Zhao, Y., 2010, October. The design of controller of buck converter. In *2010 International Conference on Computer Application and System Modeling (ICCASM 2010)* (Vol. 15, pp. V15-251). IEEE.

LIST OF PUBLICATIONS

1) Tiasha Jash, Dr. Bharat Bhushan, and Abhisekh Chaudhary, ***“Modelling and Position Control of a 3 DOF Haptic Device”*** in Proceedings of the IEEE International Conference on Energy, Power and Environment (ICEPE), NIT Meghalaya, India, 2025(*presented at conference and to be published*).

2) Tiasha Jash, Dr. Bharat Bhushan **“Intelligent Control Strategies for SEPIC Converters: A Study of PI, Fuzzy Logic, and ANFIS Techniques”** The Power and Intelligent Control Systems (PICS-2025) National institute of technology, Hamirpur.(*Accepted*)





Status of Conference Paper Submitted to PICS-2025 (Revision)

1 message

Microsoft CMT <noreply@msr-cmt.org>

To: Tiasha Jash <tiashajash123@gmail.com>

Dear Authors,

We are pleased to inform you that your paper titled "Intelligent Control Strategies for SEPIC Converters: A Study of PI, Fuzzy Logic, and ANFIS Techniques" (Submission ID: #304), has been provisionally accepted for presentation at the PICS-2025 conference, scheduled to take place from July 4-5, 2025, at NIT Hamirpur, (H.P.), India.

Kindly submit the Camera-Ready Paper by 31 May 2025, after addressing all the reviewer comments by logging in to your CMT account.

Important Notes:

[1] The Camera-Ready Paper must be strictly in the Springer Conference Paper Format (figures captions, tables, headings, references, etc.). The templates are available in the following links:

MS Word: <https://drive.google.com/file/d/1tYPp2cGK2BS4f4fB8EqpTLRvzEqIXazx/view>;

Latex: <https://www.overleaf.com/latex/templates/springer-conference-proceedings-template-updated-2022-01-12/wcvbtmwytkqj>

[2] Proofread your manuscript thoroughly to confirm that it will require no revision. The acceptance is subject to the final plagiarism and quality check and satisfactory incorporation of reviewer comments (available on the Microsoft CMT Portal) and the submission will be checked for a similarity score below 20%, as determined by plagiarism detection tools.

[3] Please note that the paper will be considered "Accepted" only after completion of the Registration and submission of the Camera-Ready Paper. The registration procedure is available in the following link: <https://pics2025nith.com/Registration>. We have added an option of hybrid mode of presentation (offline/in-person) in the registration form.

[4] Prepare a response sheet detailing how each of the reviewers' comments have been addressed. Create a file named after your Submission ID (e.g.SID402) containing the compliance report to reviewers' comments. Finally, upload this file under the Supplementary File Upload section. Kindly upload the camera-ready paper and supplementary file by 31 May 2025.

In case of any query, kindly reach out to any of the Conference Organizing Committee members.

Regards,

PICS-2025 Organizing Committee





18% Overall Similarity

The combined total of all matches, including overlapping sources, for each database.



Filtered from the Report

- Bibliography
- Quoted Text
- Cited Text

Match Groups

-  **22%** Not Cited or Quoted 18%
Matches with neither in-text citation nor quotation marks
-  **0%** Missing Quotations 0%
Matches that are still very similar to source material
-  **0%** Missing Citation 0%
Matches that have quotation marks, but no in-text citation
-  **0%** Cited and Quoted 0%
Matches with in-text citation present, but no quotation marks

Top Sources

- 7%  Internet sources
- 7%  Publications
- 15%  Submitted works (Student Papers)

Integrity Flags

0 Integrity Flags for Review

No suspicious text manipulations found.

Our system's algorithms look deeply at a document for any inconsistencies that would set it apart from a normal submission. If we notice something strange, we flag it for you to review.

A Flag is not necessarily an indicator of a problem. However, we'd recommend you focus your attention there for further review.